Title

The extrachromosomal circular DNAs of the rice blast pathogen *Magnaporthe oryzae* contain a wide variety of LTR retrotransposons, genes, and effectors

Pierre M. Joubert and Ksenia V. Krasileva

Abstract

One of the ways genomes respond to stress is by shedding extrachromosomal circular DNAs (eccDNAs). EccDNAs can contain genes and dramatically increase their copy number. They can also reinsert into the genome, generating structural variation. They have been shown to provide a source of phenotypic and genotypic plasticity in several species. However, whole-circularome studies have so far been limited to a few model organisms. Fungal plant pathogens are a serious threat to global food security in part because of their rapid adaptation to disease prevention strategies. Understanding the mechanisms fungal pathogens use to escape disease control is paramount to curbing their threat. We present a whole circularome sequencing study of the rice blast pathogen *Magnaporthe oryzae*. We find that *M. oryzae* has a highly diverse circularome containing many genes and showing evidence of large LTR retrotransposon activity. We find that genes enriched on eccDNAs in *M. oryzae* occur in genomic regions prone to presence-absence variation and that disease associated genes are frequently on eccDNAs. Finally, we find that a subset of genes is never present on eccDNAs, which indicates that the presence of these genes on eccDNAs is selected against.

Introduction

Extrachromosomal circular DNAs (eccDNAs) are a broad and poorly understood category of molecules defined simply by the fact that they are circular and originate from chromosomal DNA. This group of molecules has been referred to by many names and includes many smaller categories of molecules such as episomes, double minutes (DMs), small polydisperse circular DNAs (spcDNAs), and microDNAs. They form through several mechanisms including through non-allelic homologous recombination (HR), double strand break repair, replication slippage, replication fork stalling, R-loop formation during transcription[1], and as a byproduct of LTR retrotransposon activity[2–4] (Figure 1A). EccDNAs can accumulate in cells through autonomous replication[5,6], high rates of formation[7], or through retention in ageing cells[8]. EccDNAs can contain genes, and amplification of gene-containing eccDNAs has been linked to adaptation to copper[7] and nitrogen[5] stress in yeast, herbicide resistance[6] in weeds, and drug resistance in cancer cells[9,10]. EccDNA formation is thought to cause genomic deletions[5,11,12] and reinsertion of eccDNAs after their formation has also been thought to generate structural variation[13,14]. Some evidence also indicates that eccDNAs could facilitate horizontal gene transfer[14]. Despite their potential as important facilitators of genetic and phenotypic plasticity and presence in all eukaryotes, research efforts, and especially whole circularome sequencing experiments, have been limited to model organisms and human cancer. Therefore, how these molecules behave across the tree of life and how different species could take advantage of these molecules to rapidly adapt to their environments have remained largely unknown.

One of the greatest threats to food security is the devastation of crops by fungal plant pathogens. These pathogens secrete molecules known as effectors which modify host functions and cause disease[15]. The most promising and intensely researched solution to these diseases is the genetic modification of crops to introduce new resistance genes, often by allowing the crops to detect effectors and trigger immune

42 responses[16]. Unfortunately, the deployment of these crops has often had only short-term impacts as
43 some fungal pathogens have adapted to these defenses in very short time spans[17]. Similarly, fungicides
44 are often used to mitigate the devastation caused by these pathogens but these fungi often evolve
45 resistance to these drugs[18]. A better understanding of how these pathogens adapt and overcome
46 disease prevention efforts so quickly is vital to implementing future strategies. Sequencing and
47 characterization of the genomes of fungal plant pathogens have implicated transposable elements[19],
48 accessory chromosomes[20,21], and horizontal gene transfer[22]. Additionally, the compartmentalized
49 genome architecture of these pathogens, commonly referred to as the "two-speed" genome, is thought
50 to facilitate adaptation to stress by harboring disease associated and stress response genes in rapidly
51 evolving regions of their genomes that contain few genes and many repetitive elements[23]. However,
52 fungal plant pathogen genome evolution remains an active area of research. Given the potential for
53 eccDNAs to be a source of phenotypic and genotypic plasticity, we sought to characterize the
54 circularome of one of these pathogens to identify if eccDNAs could play a role in the rapid adaptation of
55 these organisms.

56 *Magnaporthe oryzae* (syn. *Pyricularia oryzae*) has been described as one of the most important fungal
57 pathogens threatening agriculture[24] and is the causative agent of the rice blast disease[25]. Its ease of
58 culture as well as the importance of this pathogen for global food security have propelled it to being one
59 of the most studied plant pathogens resulting in over three hundred sequenced genomes as well as
60 transcriptomic, and epigenetic datasets in addition to robust genetic tools including CRISPR/Cas9
61 mediated genome editing[26]. These tools and datasets make *M. oryzae* a prime candidate for
62 understanding the role eccDNAs may play in adaptation to stress in a fungal plant pathogen.

63 We present here our analysis of circularome sequencing data for *M. oryzae* and identify eccDNA forming
64 regions in its genome. We describe the high diversity of eccDNA forming regions that we found in the
65 rice blast pathogen and compare it to previously sequenced circularomes. We find that most of the *M.*
66 *oryzae* circularome is made up of LTR retrotransposon sequence and that genes on eccDNAs tend to
67 originate from regions of the genome prone to presence-absence variation. Additionally, our
68 characterization of the genes found on eccDNAs suggests that many genes are never found on eccDNAs,
69 and that selection may shape which genes are found on these molecules. Finally, our analysis reveals
70 that many disease-causing effectors are found on eccDNAs in the pathogen.

71 **Results**

72 **Identification of eccDNA forming regions in *Magnaporthe oryzae***

73 To characterize the circularome of *M. oryzae*, eccDNAs were purified and sequenced from pure cultures
74 of *M. oryzae* Guy11 using a protocol adapted from previously published methods[27]. Briefly, after total
75 DNA extraction, linear DNA was degraded using an exonuclease and the remaining circular DNA was
76 amplified using rolling circle amplification (RCA). Depletion of linear DNA was verified using qPCR and
77 primers to the *M. oryzae* actin gene which has previously been used as a marker for linear DNA since
78 increased copies of the ACT1 gene are thought to be deleterious in yeast[28,29] (Supplemental Figure 1).
79 Isolated eccDNAs were then sequenced using both paired-end Illumina sequencing and PacBio circular
80 consensus sequencing (CCS).

81 To identify eccDNAs from our Illumina sequencing data, we developed a pipeline inspired by previously
82 published methods[11]. In circularome sequencing data, split mapping reads often originate from
83 sequencing of circularization junctions of eccDNAs and opposite facing read pairs represent sequencing

from paired-end sequencing fragments that span these circularization junctions. Our pipeline uses split reads in combination with opposite facing read pairs to find evidence of eccDNA formation. This allowed us to identify, with high confidence, genomic sequences belonging to eccDNAs, which we will hereafter refer to simply as "eccDNA forming regions." We will refer to split reads associated with these eccDNA forming regions simply as "junction split reads." Across all 8 sequenced samples, our pipeline identified 1,719,878 eccDNA forming regions using our Illumina paired-end sequencing data (Supplemental Data File 1).

We also inferred eccDNA forming regions using our PacBio sequencing data. This was done using a similar pipeline with less stringent criteria which was necessary given the much lower coverage of this sequencing data. This sequencing data allowed us to identify 147,335 eccDNA forming regions across all samples (Supplemental Data File 2). We compared these eccDNA forming regions to those called using Illumina data and found that, on average, 81.42% of eccDNA forming regions called using PacBio data for one sample were also found in our eccDNA forming regions called using Illumina reads in the same sample (Supplemental Figure 2). We were able to attribute much of this discrepancy to our stringent criteria for calling eccDNA forming regions since simply looking for split reads in our Illumina data increased this rate to 90.36% (Supplemental Figure 2). The remaining differences are likely due to Illumina reads not being long enough to properly be mapped as split reads in certain regions of the genome. Aside from this validation, we chose not to include the PacBio data in our final analyses due to the lower read coverage.

Next, we quantified the potential false positive rate of our pipeline by running it on previously published whole genome sequencing data from *M. oryzae*[26,30,31]. Based off the number of eccDNA forming regions called from this data, we estimated this false positive rate at less than 3 junction split reads per million sequencing reads (Supplemental Table 1). For comparison, we found 38,585 junction split reads per million reads in our samples on average which indicates that the false positive rate of our pipeline is very low. Additionally, we could not rule out the presence of eccDNAs in the whole genome sequencing data we analyzed.

Finally, we compared previously published eccDNA forming regions in human tissue[11] to the output from our pipeline using the same data. This comparison showed that, on average, 74.62% of eccDNA forming regions called by our pipeline were also found in the published dataset (Supplemental Figure 3A). This number was even higher for eccDNA forming regions associated with 10 or more junction split reads (85.63%). The small fraction of eccDNA forming regions called by our pipeline that did not appear in the published list could not be attributed to how our pipeline handled multi-mapping reads (see Methods) and were likely due to differences in sequence data processing and different criteria for selecting split reads[11] (Supplemental Figure 3).

However, the two lists significantly differed in the number of eccDNA forming regions identified, with our pipeline identifying substantially less (Supplemental Figure 3B). This difference can be attributed to our stricter evidence to call eccDNA forming regions. In our method, eccDNA forming regions were only called if split reads mapped to the region. This is in contrast to other methods of calling eccDNA forming regions which sometimes relies purely on peaks in sequencing coverage[11,28]. This meant that our pipeline could not detect eccDNAs formed from HR between identical repeats which do not result in split mapping reads. We chose this method for *M. oryzae* because it showed circularome sequencing coverage throughout the entire genome in our samples and very few clear coverage peaks. Regardless,

126 the high degree of overlap between our called eccDNA forming regions and those described by Møller et
127 al. makes us confident that the eccDNA forming regions we called using our pipeline are robust.

128 **The *M. oryzae* circularome is more diverse and contains more noncoding sequences than the**
129 **circularomes of other organisms**

130 We were first interested in comparing the circularome of *M. oryzae* to those of other previously
131 characterized organisms. To compare these datasets across different organisms, we gathered
132 sequencing data from several previous studies[11,27,28,32] and reanalyzed them using our pipeline
133 (Supplemental Data Files 3-18). This analysis revealed a very large number of eccDNA forming regions in
134 *M. oryzae* compared to other previously sequenced organisms (Figure 1B). This result was still striking
135 after normalizing for genome size and sequencing library size (Supplemental Figure 4A). While this
136 difference could be attributed to differences in the methods used for eccDNA purification, our own
137 eccDNA samples extracted from *Oryza sativa* had similar levels of diversity to previously sequenced
138 samples (Supplemental Table 2). Additionally, *M. oryzae* had more eccDNA forming regions made up of
139 noncoding sequences relative to the percentage of noncoding sequence in its genome than other
140 organisms aside from *S. cerevisiae* (Figure 1B, Supplemental Figure 4B).

141 **LTR retrotransposon sequences make up most of the *M. oryzae* circularome**

142 LTR/Gypsy and LTR/Copia retrotransposons frequently generate eccDNAs through several mechanisms[2–
143 4], so we looked for the presence of these sequences in the *M. oryzae* circularome. Our analysis revealed
144 that 54.12% of the eccDNA forming regions we identified seemed to be composed of more than 90%
145 LTR retrotransposon sequence indicating that these elements made up a large portion of the pathogen's
146 circularome. Further comparative analysis revealed that a much higher proportion of the *M. oryzae*
147 circularome was made up of these LTR retrotransposon sequences than in other organisms (Figure 1B,
148 Supplemental Figure 4C and 4D). Additionally, this analysis also showed that the epigenetic regulation
149 mutant *A. thaliana epi12* had an increased portion of its circularome made up by LTR/Copia sequences
150 as previously described[27] which supports our re-analysis approach (Supplemental Figure 4D).

151 All six LTR retrotransposons identified in *M. oryzae* Guy11 formed eccDNAs (Figure 2A). However, the
152 elements MAGGY, GYMAG1, and Copia1 made up the majority of eccDNA sequencing data (Figure 2B).
153 When this data was normalized to the proportion of the genome made up by each transposon, GYMAG1
154 stood out as making up a much greater percentage of the sequencing data than expected (Figure 2C,
155 Supplemental Figure 5).

156 **LTR retrotransposon in *M. oryzae* form eccDNAs through a variety of mechanisms**

157 LTR retrotransposons can form eccDNAs through a variety of mechanisms[2–4]. EccDNA formation
158 commonly occurs after transcription and reverse transcription of the transposon which results in a linear
159 fragment of extrachromosomal DNA[33] (Figure 1A). The most common of these mechanisms are through
160 nonhomologous end joining (NHEJ) of the two LTR ends to form eccDNAs containing 2 LTRs (scenario 1,
161 Figure 3A), autointegration of the retrotransposon forming single LTR eccDNAs of various lengths,
162 depending on where in the internal sequence of the transposon the autointegrations happens (scenario
163 2, Figure 3B), HR between the two LTRs to form single LTR eccDNAs (scenario 3, Figure 3C). Finally, LTR
164 retrotransposons sequences can also become part of eccDNAs by other eccDNA formation mechanisms
165 that do not rely on transposon activity, such as intrachromosomal HR between solo-LTRs or multiple

166 copies of the same transposon[4,5,28]. Given this diversity of mechanisms, we wanted to identify whether
167 there were differences across LTR retrotransposons in *M. oryzae* in their tendency to form through one
168 mechanism or another. To this end, we first simulated the expected read coverage for each of the three
169 active LTR eccDNA formation mechanisms under ideal conditions where only one mechanism of
170 formation was occurring (Figure 3A-C). Furthermore, we also measured the prevalence of scenarios 1
171 and 2 by identifying specific split read variants. LTR eccDNAs formed through NHEJ result in split reads
172 that map to one end of an LTR and the other which we will refer to as LTR-LTR split reads (Supplemental
173 Figures 6 and 8A). Autointegration results in split reads that map to one LTR and to the internal region of
174 the transposon which we will refer to as LTR-internal split reads (Supplemental Figure 7, 8B). HR
175 between two identical LTRs (scenario 3) would not result in a split read so we could not find this type of
176 evidence in our data.

177 Combining and interpreting this data gave us some insights into the mechanisms through which each
178 LTR retrotransposon forms eccDNAs. For example, the shape of the profile plot for the observed read
179 coverage for MAGGY indicated that it forms eccDNAs primarily through autointegration (Figure 3D). This
180 was supported by a high correlation between the number of sequencing reads and LTR-internal split
181 reads for MAGGY (Supplemental Figure 6) and a low correlation between sequencing reads and LTR-LTR
182 split reads (Supplemental Figure 7). The data also pointed to MGRL3 and GYMAG1 forming eccDNAs
183 primarily through autointegration (Figure 3E, 3G, Supplemental Figures 6 and 7). Copia1, on the other
184 hand showed a clear pattern of read coverage corresponding to eccDNA formation through HR (Figure
185 3F), though the high correlation between sequencing reads and LTR-internal split reads mapping to this
186 element hinted that a small, but proportional, fraction of Copia1 elements formed eccDNAs through
187 autointegration (Supplemental Figure 7). In the case of GYMAG2, its sequencing read coverage
188 resembled a pattern expected for LTR-eccDNAs formed through NHEJ (Figure 3H). The large amount of
189 LTR-LTR split reads found corresponding to GYMAG2 elements compared to other retrotransposons
190 supported this inference (Supplemental Figure 8). Finally, PYRET's distinct sequencing read coverage
191 profile likely indicated that it mostly formed eccDNAs passively (Figure 3I). A low correlation between
192 sequencing read coverage and both LTR-LTR split reads and LTR-internal split reads as well as the
193 fragmented nature of PYRET elements which is a sign of low recent retrotransposon activity, supported
194 this inference (Supplemental Figures 6 and 7).

195 **MicroDNAs are distinct from other eccDNAs**

196 MicroDNAs have previously been studied as a distinct set of molecules within the eccDNA category.
197 Besides being small (less than 400bp), microDNAs are found to be enriched in genic regions, exons,
198 5'UTRs and CpG islands[12,34]. We examined if microDNAs in *M. oryzae* showed these characteristics by
199 analyzing eccDNA forming regions less than 400 bp in length with less than 10% LTR retrotransposon
200 sequence across different organisms. Enrichment of microDNAs in CpG islands was the most consistent
201 across all organisms though this enrichment was not found in in *M. oryzae* (Supplemental Figure 9).
202 Similarly, we found no enrichment of microDNAs in 5'UTRs in *M. oryzae*. We did however find a small
203 enrichment of microDNAs in genic regions in *M. oryzae* as in many of the other sequenced organisms
204 (Supplemental Figure 9 and 10). In general, our analysis suggested that the previously described
205 characteristics of microDNAs are not common across all organisms and sample types.

206 MicroDNAs also displayed distinct features from the remaining subset of non-LTR eccDNAs which we
207 called large eccDNAs. Among other differences, we found that, unlike microDNAs, large eccDNAs tended

208 to be enriched in intergenic regions (Supplemental Figures 10 and 11). Additionally, eccDNAs are often
209 associated with active transcription[1,7], and we found a slight but significant correlation between
210 expression and junction split reads for large eccDNAs but not for microDNAs (Supplemental Figure 12).

211 In yeast, eccDNA amplification is thought to often occur with the help of autonomously replicating
212 sequences (ARSs) which contain ARS consensus sequences (ACSs)[5,28,35]. In *M. oryzae*, we found that ACSs
213 were enriched in large eccDNAs (permutation test, mean of expected: 5320.14 regions, observed: 6950
214 regions, $p < 0.01$, n = 100 replicates) but depleted in microDNAs (permutation test, mean of expected:
215 818.09 regions, observed: 714 regions, $p < 0.01$, n = 100 replicates). However, for both large eccDNAs
216 and microDNAs, presence of an ACS in the eccDNA forming region did not result in an increased number
217 of junction split reads (Supplemental Figure 13).

218 Finally, microDNAs have been found to be associated with active chromatin marks and increased GC
219 content[12,34]. However, we did not find any of these enrichments in microDNAs or large eccDNAs in *M.*
220 *oryzae* (Supplemental Figure 14).

221 **Many genes are found encompassed by eccDNA forming regions**

222 Many eccDNAs contain genes and these eccDNAs can provide genotypic and phenotypic plasticity in
223 other organisms. In *M. oryzae* we found that, out of the 12,115 genes in Guy11, 9,866 were fully
224 contained in an eccDNA forming region in at least one sample. These genes included TRF1 and PTP2
225 which have been shown to be involved in fungicide resistance in *M. oryzae*[36,37]. However, not all genes
226 were observed in eccDNA forming regions at the same frequency. To further understand what types of
227 genes are enriched in eccDNA forming regions, we selected a set of eccDNA-associated genes. This set
228 was identified by first scoring each gene by the number of junction split reads that fully encompassed
229 that gene. 986 genes that were in the top 10% of genes for this score were selected (Figure 4A,
230 Supplemental Data File 19). We referred to this score as the number of "encompassing split reads" for
231 each gene. We then performed gene ontology (GO) enrichment analysis and found that eccDNA-
232 associated genes were enriched for GO terms related to vesicle trafficking among other terms (Figure
233 5A, Supplemental Figure 15, Supplemental Data Files 20-22).

234 **EccDNA-associated genes are found in gene sparse and repeat dense regions of the genome**

235 Some plant pathogens are described as having 'two-speed' genomes with housekeeping genes found
236 close together in repeat-poor regions and environmentally responsive and disease-associated genes
237 found in repeat-dense and gene-poor regions. To determine if eccDNA-associated genes were enriched
238 in either of these genomic contexts, we analyzed if eccDNA-associated genes were more distant from
239 other genes than expected by chance (Figure 6). We observed a significant difference (permutation test
240 for difference of medians, $p < 0.0001$, n = 10,000 replicates) between the median distance to the nearest
241 gene of eccDNA-associated genes (593 base pairs) and other genes (478 base pairs). We also observed a
242 significant difference (permutation test for difference of medians, $p = 0.0007$, n = 10,000 replicates)
243 between the median distance to the nearest genomic repeat of eccDNA-associated genes (649 base
244 pairs) and other genes (776 base pairs, Supplemental Figure 16). This difference in proximity was not
245 observed for transposable elements specifically indicating that transposable elements alone were not
246 responsible for this effect (Supplemental Figure 17).

247 **EccDNA-associated genes are prone to presence-absence variation**

248 There is evidence of eccDNAs generating structural variation in other organisms[13,14]. We therefore
249 tested whether eccDNA formation is associated with genes prone to presence-absence variation in 162
250 rice-infecting *M. oryzae* isolates (Supplemental Data File 25). As expected from previous studies[38,39], our
251 analysis indicated that predicted effectors were more likely to experience presence-absence variation
252 (Supplemental Figure 18; X-squared = 146.33, df = 1, p-value < 2.2e-16). We also found that eccDNA-
253 associated genes were more likely to be prone to presence-absence variation (Figure 4B and
254 Supplemental Data File 19; X-squared = 28.511, df = 2, p-value = 6.44e-07). This result suggested that
255 eccDNA formation and structural variation occur in similar regions of the genome but did not show
256 whether they are directly linked.

257 To see if a more direct link existed, we surveyed the genomes of the *M. oryzae* isolates for small
258 deletions that completely or partially overlapped genes but did not disrupt neighboring genes. We were
259 able to identify 257 such events (Supplemental Data File 24). However, none of these deletions matched
260 our eccDNA forming regions and only 8 of them came within 50 bp. This result was unlikely to be
261 conclusive though given that rarefaction analysis for both large eccDNAs and microDNAs revealed that
262 there is likely to be a much greater diversity of these molecules than what we were able to capture at
263 the sequencing depth of this study (Supplemental Figure 19).

264 Similarly, we were interested in identifying any potential DNA translocations that may have occurred
265 through an eccDNA intermediate. While we were able to successfully construct a pipeline that identified
266 one previously described eccDNA-mediated translocation in wine yeast[14] (Supplemental Figure 20), we
267 were unable to identify any such examples in any of the *M. oryzae* genomes we analyzed despite
268 including isolates infecting a variety of hosts in this analysis (306 genomes in total, Supplemental Data
269 File 25).

270 Finally, since mini-chromosomes have been hypothesized as playing important roles in fungal plant
271 pathogen evolution, we also sought to determine whether genes that were previously found on *M.*
272 *oryzae* mini-chromosomes were associated with eccDNA formation but found no such effect
273 (Supplemental Figure 21).

274 **Many genes that are never found on eccDNAs are cytoskeleton-related**

275 Since most *M. oryzae* genes appeared in eccDNA forming regions in at least one sample, we were
276 particularly interested in the 2,249 eccDNA-absent genes (Supplemental Data File 19). We first verified
277 that eccDNA-absent genes were not due to insufficient sequencing coverage using rarefaction analysis.
278 Given the high coverage of our data, we only expected to find approximately 468 genes in this category
279 by chance (Figure 4C).

280 We next explored whether gene expression or other genomic markers could explain the genes in this
281 category. However, we found no difference between eccDNA-associated genes and eccDNA-absent
282 genes in gene expression, GC content, or histone marks aside from a slight difference in H3K36me3
283 (Supplemental Figure 22 and 23).

284 Finally, we performed GO enrichment analysis on these genes and found, amongst many other enriched
285 terms, that terms related to cytoskeletal proteins were enriched within eccDNA-absent genes (Figure
286 6B, Supplemental Figure 24, Supplemental Data Files 26-28). This result is of particular interest given
287 that cytoskeletal genes, specifically the actin gene, have been used in a previous study[28] as well as this

one, as a marker for linear DNA due to its negative fitness effect at high copy numbers in yeast[29]. This suggested that certain groups of genes may be protected from eccDNA formation or maintenance of these eccDNAs in the cell.

Effectors are enriched in eccDNA forming regions compared to other genes

Next, we wanted to identify whether eccDNA forming regions contained disease-causing effectors. We found that many known *M. oryzae* effectors were encompassed by eccDNA forming regions in at least one sample. This included *AvrPita3*, *AvrPita1*, *AvrPi9*, *AvrPi54*, *AvrPiz-t*, and *Pwl4* (Figure 7A, Supplemental Data File 19). Additionally, we found that many predicted effectors were found in eccDNA forming regions (Figure 7B, Supplemental Data File 19). We also found that many of these putative effectors were associated with large numbers of encompassing split reads and found this difference to be statistically significant (Figure 7C; permutation test for difference in medians, $p < 0.0001$, $n = 10{,}000$ replicates). Effectors are often small genes and, given the often-small size of eccDNA forming regions in our data, we felt that our analysis could be affected by this bias. To address this issue, we repeated our permutation test, comparing predicted effectors to a set of non-effectors of similar lengths and again found a significant difference in number of encompassing split reads (permutation test for difference in medians with correction for gene length distribution, $p = 0.0206$, $n = 10{,}000$ replicates). This result suggests that effectors are more likely to be found on eccDNAs than other genes in *M. oryzae* and that effect is not simply due to their size.

Discussion

EccDNAs have been shown to be a potential source of significant phenotypic[5–7,9,10] and genotypic[13,40] plasticity that can help organisms adapt to stress. While eccDNAs have been extensively studied in human cancer[1], very few studies have attempted to study the circularome of other organisms, and even fewer have generated high quality whole circularome sequencing data. To expand our understanding of eccDNAs across the tree of life, we studied the circularome of the fungal plant pathogen *M. oryzae* and, through this analysis, developed many tools to analyze whole circularome sequencing data which can often be difficult to interpret. These include a new pipeline to identify eccDNA forming regions and frameworks for comparing this data across organisms, identifying mechanisms of eccDNA formation of LTR retrotransposons, identifying gene sets enriched or depleted in eccDNAs, and identifying structural variants that may have been caused by eccDNAs. Our analysis also revealed that the circularome of *M. oryzae* contains a wide diversity of eccDNA forming regions that appeared to exceed those of other previously characterized organisms. We also found that eccDNA forming regions in *M. oryzae* were more commonly made up LTR retrotransposons than other organisms. These differences highlight the need to further characterize the circularome of other organisms as the current datasets are clearly not representative of all organisms.

We analyzed the types of genes that were found on eccDNAs in *M. oryzae* and found that eccDNA-associated genes were often prone to presence-absence variation, hinting at a link between eccDNAs and genomic plasticity. However, we could not find direct evidence of gene deletions occurring through an eccDNA intermediate in *M. oryzae*. Similarly, we could not find any evidence of eccDNA-mediated translocations. These results could be due to our sequencing coverage and our bioinformatics pipelines not showing the full diversity of eccDNAs in *M. oryzae*. Our scripts were able to identify an eccDNA-mediated translocation in wine yeasts but were limited to non-repetitive regions of the genome and may have missed some of these events in *M. oryzae*. Additionally, it is possible that eccDNA-mediated

translocations occur on a larger time scale than what we were able to sample within the *M. oryzae* species. However, it is likely that experimental approaches including inducing eccDNA formation in the lab are necessary to determine whether these events lead to chromosomal deletions or rearrangements. On a genome-wide scale, single cell sequencing of the circularome as well as genomic DNA could also lead to a more precise view of eccDNA formation and structural variation as they occur in the cell during vegetative growth.

We found some evidence that suggests that eccDNA formation could be a potential mechanism for phenotypic plasticity in *M. oryzae*. For example, we identified two genes associated with fungicide resistance in our eccDNA forming regions. We found that eccDNA-associated genes presented characteristics associated with the gene-sparse, repeat-rich, and "fast" part of the plant pathogen genome where rapid adaptation to stress occurs[23]. The fact that eccDNA-associated genes were closer to repeats than other genes but not transposons specifically indicates that this effect was not simply caused by eccDNA formation by LTR retrotransposons. We also specifically found that predicted effectors were more commonly found fully encompassed by eccDNA forming regions than expected by chance. This result could be simply driven by the genomic context in which eccDNAs are commonly formed but could also point to eccDNAs playing a role in the evolution of these important genes.

Additionally, we identified a set of eccDNA-absent genes that were not explained simply by incomplete sequencing. The existence of this group of genes hints at selective pressure acting on eccDNA formation and preventing genes that are deleterious at increased copy numbers, such as cytoskeletal proteins, from accumulating high copy numbers through eccDNA formation. On the other hand, selective pressure caused by growth under stress conditions could favor *M. oryzae* cells containing higher copy numbers of genes important for survival under these conditions as has been extensively shown in other organisms[5–7,9,10]. This could be caused either by extrachromosomal replication of eccDNAs, which the enrichment of ACSs in our eccDNA forming regions hinted at, or by high rates of formation either through random asymmetric segregation of eccDNAs at mitosis, as has been shown in cancer[10], or through retention of eccDNAs in ageing cells as has been shown in yeast[8]. Further experimentation and characterization of the *M. oryzae* circularome under stress is necessary to investigate if this eccDNA-mediated phenotypic plasticity is present in the plant pathogen. We attempted to perform such experiments by sequencing *O. sativa* tissue infected by *M. oryzae* but found that rice eccDNAs crowded out the circularome sequencing signal and prevented meaningful analysis.

In conclusion, this study begins the characterization of the *M. oryzae* circularome and highlights its potential for generating phenotypic and genotypic plasticity. If eccDNAs were to facilitate these phenomena, they could become potential drug targets to prevent the rapid adaptation of the blast pathogen to environmental stress, fungicides, and resistant crop varieties. Furthermore, regions and genes prone to forming eccDNAs could be excluded as drug targets or as targets for engineered resistance in crops. On the other hand, we found 1,820 genes including several predicted effectors in the *M. oryzae* genome that were present in all other rice infecting isolates that we analyzed and that were in the eccDNA-absent group. These genes could be high potential targets for drug design or engineered resistance. Nevertheless, eccDNAs remain largely underexplored, especially in fungal plant pathogens, and, given their potential, further characterization of this circularome, especially under stress, is likely to prove valuable. Furthermore, this study presents a characterization of the circularome of a single fungal plant pathogen, and it will be important to perform a broader survey of these organisms to fully understand the role of eccDNAs in their adaptation to stress.

373 **Methods**

374 ***M. oryzae* growth and DNA extraction**

375 *M. oryzae* Guy11 was grown on Difco oatmeal agar plates for 21 days under constant light in a Percival
376 Scientific Incubator Model CU-36L4 equipped with half fluorescent lights and half black lights. 1 cm^2 of
377 mycelium was scraped from the colony edge and used to start 3 liquid cultures (biological replicates) in
378 15 ml complete medium[41] (CM) in petri dishes. Liquid cultures were incubated without shaking for 3
379 days in the same growth chamber.

380 Total DNA extraction was performed according to a protocol from the Prof. Natalia Requena group at
381 the Karlsruhe Institute of Technology. Briefly, mycelium grown in liquid culture was washed 3 times with
382 water and then ground in liquid nitrogen. Ground mycelium was incubated in extraction buffer (0.1M
383 Tris-HCl pH 7.5, 0.05 M EDTA, 1% SDS, 0.5 M NaCl) at 65°C for 30 minutes. 5M potassium acetate was
384 then added to the samples which were then incubated on ice for 30 minutes. The supernatant was then
385 washed with isopropanol and ethanol. Finally, the DNA pellet was resuspended in water and treated
386 with RNase A (Thermo Scientific).

387 ***O. sativa* growth and DNA extraction**

388 *O. sativa* samples were originally intended to serve as control samples to be compared to tissue infected
389 by *M. oryzae* and therefore the methods below reflect this original intent. However, circularome
390 sequencing data obtained from infected tissue was not included in this study as it included very little
391 sequencing data that mapped to the *M. oryzae* Guy11 genome.

392 *O. sativa* cv. Nipponbare seeds were surface sterilized in 70% ethanol for 1 minute and 10% bleach for
393 10 minutes with thorough rinsing in sterile water after each before being placed on wet filter paper in a
394 petri dish. The petri dish was wrapped in foil and placed at 4°C for 2 days to germinate. Germinated
395 seedlings were planted in potting mix made up of 50% Turface and 50% Super Soil. Seedlings were
396 grown for three weeks in a greenhouse under standard conditions. For each of three biological
397 replicates, the first true leaf was cut from one rice plant, its tip was removed, and it was then cut into
398 two equal segments, approximately 10mm in length. This pair of segments was then placed on their
399 abaxial surface on wet filter paper in a petri dish. Five hole-punches of filter paper soaked in 0.25%
400 gelatin and 0.05% Tween-20 were then placed on each segment. The petri dishes were then placed in an
401 airtight container with wet paper towels and placed on a windowsill for 7 days. Hole-punches were
402 removed and non-chlorotic tissue in contact with hole-punches was ground in liquid nitrogen. DNA
403 extraction was then performed using the Qiagen Plant DNeasy mini kit.

404 **Circular DNA enrichment**

405 Total DNA obtained from biological replicates was then split into three technical replicates before
406 circular DNA enrichment. This enrichment was performed according to a protocol from Lanciano et al.
407 with a few modifications[27]. To purify the samples and begin removing large linear DNA fragments, the
408 samples were treated using a Zymo Research DNA Clean and Concentrator kit and standard protocols.
409 Linear DNA digestion was then performed using Epicentre PlasmidSafe DNase and incubated at 37°C for
410 24 hours. DNase, ATP, and reaction buffer were then added to the samples every 24 hours while the
411 incubation continued. In total, the reaction was allowed to proceed for 96 hours. Remaining DNA was
412 then precipitated overnight at 4°C by adding 0.1 volume 3M sodium acetate, 2.5 volumes ethanol and 1

413 ul glycogen (20 mg/ml). Rolling circle amplification was then performed using the Illustra TempliPhi 100
414 Amplification Kit (GE Healthcare). Precipitated DNA was resuspended directly in 20 ul of the Illustra
415 TempliPhi sample buffer and the amplification reaction was allowed to proceed for 24 hours at 30°C.

416 **Verification of circular DNA enrichment**

417 In a separate experiment, 5 samples of *M. oryzae* mycelium were grown up in liquid culture and total
418 DNA was extracted. Circular DNA enrichment was performed as before with some exceptions and
419 without technical replicates. First, linear DNA digestion was only performed for 72 hours for 3 samples.
420 Second, aliquots of the incubating samples were taken at 0 hours, 24 hours, 48 hours and 72 hours for
421 these 3 samples, and 0 hours, 48 hours, 72 hours and 96 hours for the last 2 samples. qPCR was then
422 used to verify linear DNA depletion in each sample using an Applied Biosystems QuantStudio 5
423 instrument and the QuantStudio Design and Analysis desktop software. Primers 5'-
424 GTATGTGCAAGGCCGGTTTC-3' and 5'- GCACATCTGTCGACAAACCG-3' were used to amplify the *M. oryzae*
425 actin gene (MGG_03982) along with Lightcycler 480 Sybr Green I master mix. Data from four qPCR
426 technical replicates was obtained. Remaining linear DNA fraction in each sample at each timepoint was
427 then calculated using the $2^{-\Delta\Delta Ct}$ method.

428 **Illumina library preparation and sequencing**

429 Library preparation was performed by the QB3-Berkeley Functional Genomics Laboratory at UC
430 Berkeley. DNA was fragmented with an S220 Focused-Ultrasonicator (Covaris), and libraries prepared
431 using the KAPA Hyper Prep kit for DNA (Roche KK8504). Truncated universal stub adapters were ligated
432 to DNA fragments, which were then extended via PCR using unique dual indexing primers into full length
433 Illumina adapters. Library quality was checked on an Agilent Fragment Analyzer. Libraries were then
434 transferred to the QB3-Berkeley Vincent J. Coates Genomics Sequencing Laboratory, also at UC Berkeley.
435 Library molarity was measured via quantitative PCR with the KAPA Library Quantification Kit (Roche
436 KK4824) on a BioRad CFX Connect thermal cycler. Libraries were then pooled by molarity and sequenced
437 on an Illumina NovaSeq 6000 S4 flowcell for 2 x 150 cycles, targeting at least 10Gb per sample. Fastq
438 files were generated and demultiplexed using Illumina bcl2fastq2 version 2.20 and default settings, on a
439 server running CentOS Linux 7. One technical replicate did not pass quality control before library
440 preparation and was omitted.

441 **PacBio library preparation and sequencing**

442 Using a Covaris S220 Focused-Ultrasonicator, 2 ug of each DNA sample was sheared to an approximate
443 fragment size of 5000 bp and purified using AMPure XP beads (Beckman Coulter). Library preparation
444 was performed using the NEBNext Ultra DNA Library Prep Kit (kit number E7370L, New England Biolabs)
445 and 8 cycles of PCR. Libraries were then quality controlled using a Bioanalyzer high sensitivity DNA chip
446 and the Agilent 2100 Bioanalyzer system. One technical replicate did not pass quality control before
447 library preparation and was omitted. The samples were then submitted to Novogene (Tianjin, China) for
448 PacBio sequencing which was performed on the PacBio Sequel platform using a 60-minute sequencing
449 strategy.

450 **Inferring eccDNA forming regions from short read sequencing data**

451 Illumina sequencing signal was analyzed using a custom pipeline inspired by previously published
452 methods[11]. Illumina reads were first trimmed of Illumina TruSeq adapters using CutAdapt[42] version 2.4

with the nextseq-trim=20 option. Trimmed reads were then mapped to the *M. oryzae* Guy11 genome[43] and the 70-15 mitochondrial sequence[44] obtained from the Broad Institute (https://www.broadinstitute.org/scientific-community/science/projects/fungal-genome-initiative/magnaporthe-comparative-genomics-proj) using BWA-MEM[45] version 0.7.17-r1188 and the q and a options. Reads mapping to mitochondrial sequences were excluded. Uniquely mapped reads were then mined for split reads that mapped in the same orientation, had at least 20 bp of alignment on either side of the split, mapped to only two places in the genome, and where the start of read mapped downstream from the end. This last filter sets these split reads apart from split reads that would indicate a deletion in the genome. Split reads where one side mapped more than 50kbp away from the other or to a different scaffold than the other were excluded. Opposite facing read pairs were also obtained from uniquely mapped reads. Candidate eccDNA forming regions were then inferred by combining these two structural read variants. A split read that contained an opposite facing read pair that mapped no more than a combined 500 bp from the borders of the region contained within the two halves of the split read was considered a candidate eccDNA and a junction split read. The length distribution of these candidate eccDNA forming regions (Supplemental Figure 25A) was then used to probabilistically infer candidate eccDNA forming regions from multi-mapping reads (Supplemental Figure 25B). For each multi-mapping split read, a list of potential combinations of alignments that satisfied the previously described criteria for split reads was generated and one of these combinations was chosen at random, weighted by their length according to the generated length distribution. The chosen combinations were then used to infer additional candidate eccDNA forming regions by combining these with opposite facing read pairs as before, except this time obtained from multi-mapping reads.

Each candidate eccDNA forming region was then validated by verifying that the region had over 95% read coverage and at least two junction split reads with the exact same coordinates. Candidate eccDNA forming regions that did not pass these criteria were considered low quality and were not included in the analysis.

Inferring eccDNA forming regions from long read sequencing data

Circular consensus sequences (CCS) were first called from PacBio data using ccs version 3.4.1 (https://ccs.how/). Demultiplexing was then performed using lima version 1.9.0 (https://lima.how/). CCSs were then mapped to the *M. oryzae* Guy11 genome using minimap2[46] version 2.18-r1015. Only uniquely mapped reads were kept for analysis. We then identified eccDNA forming regions by looking for split reads that either mapped to the same orientation to the same exact region multiple times or pairs of split alignments that were less than 50 kb apart, mapped in the same orientation and oriented properly so that they were indicative of a circular junction rather than a deletion.

Comparing eccDNA forming regions inferred from Illumina data and eccDNA forming regions inferred from PacBio data

EccDNA forming regions called using Illumina data and PacBio data were found to be identical if their start and end coordinates were within 10 bp of each other. EccDNA forming regions were then called with less stringent requirements to verify if any of the missing eccDNA forming regions were being filtered out somewhere in the pipeline. In this test, all uniquely mapped split reads that had 10 or more bp overlap on either side, were properly oriented, and were less than 50kb apart were considered eccDNA forming regions.

494 **Comparing the eccDNA forming regions called using our pipeline to a previously published pipeline**

495 EccDNA forming regions called using our pipeline were compared to eccDNA forming regions previously
496 published for *H. sapiens*[11]. EccDNA forming regions were found to be identical if their start and end
497 coordinates were within 10 bp of each other. EccDNA forming regions described as low quality by the
498 authors were excluded from the published dataset before comparison. High coverage eccDNA forming
499 regions were chosen for comparison if they had more than 10 associated junction split reads. Finally,
500 multi-mapping reads were excluded from the pipeline to identify eccDNA forming regions called using
501 only uniquely mapped reads.

502 **Gene annotation**

503 The *M. oryzae* Guy11 genome along with 162 other rice-infecting *M. oryzae* genomes (Supplemental
504 Data File 23) were annotated using the FunGAP[47] version 1.1.0 annotation pipeline. For all genomes,
505 RNAseq data (SRR8842990) obtained from GEO accession GSE129291 was used along with the
506 proteomes of *M. oryzae* 70-15, P131 and MZ5-1-6 (accessions GCA_000002495.2, GCA_000292605.1,
507 and GCA_004346965.1, respectively) taken from GenBank. The 'sordariomycetes_odb10' option was
508 used for the busco_dataset option and the 'magnaporthe_grisea' option was used for the
509 augustus_species option. For repeat masking, a transposable element library generated by combining
510 the RepBase[48] fngrep version 25.10 with a *de novo* repeat library generated by RepeatModeler[49] version
511 2.0.1 run on the *M. oryzae* Guy11 genome with the LTRStuct argument was used for all genomes. Genes
512 in *M. oryzae* Guy11 were assigned names according to the gene names listed on UniProtKB for *M.*
513 *oryzae* 70-15. To make this assignment, *M. oryzae* Guy11 proteins were aligned to the *M. oryzae* 70-15
514 proteome using BLASTP[50] version 2.7.1+ and hits with greater than 80% sequence identity and that
515 spanned more than 80% of the length of both the *M. oryzae* Guy11 protein and the *M. oryzae* 70-15
516 protein were kept.

517 **High quality LTR-retrotransposon annotations in *M. oryzae***

518 High quality, full length, consensus sequences for known LTR/Gypsy elements in *M. oryzae* (MAGGY,
519 GYMAG1, GYMAG2, PYRET, MGRL3) and one LTR/Copia element (Copia1) were generated using the
520 WICKERsoft[51] suite of tools. Reference sequences from other genomes for each element were obtained
521 from the RepBase[48] fngrep version 25.10 library. The *M. oryzae* Guy11 genome was then screened for
522 the presence of these sequences using BLASTN[50] version 2.2.9 and then filtered to hits with 90%
523 sequence identity and that contained 90% of the sequence length. Hits for each reference sequence
524 were then extended to include 500 base pairs of genomic sequence upstream and downstream of the
525 hit. A multiple sequence alignment of hits for each reference sequence was then generated using
526 ClustalW[52] version 1.83 and boundaries were visually inspected and trimmed. Consensus sequences for
527 each element were then generated from these multiple sequence alignments. These consensus
528 sequences were split into LTR and internal regions by self-alignment using the BLASTN[50] webserver in
529 August 2020 to identify LTRs. These consensus sequences are available in Supplemental Data File 29.
530 Finally, the locations of these elements in *M. oryzae* Guy11 genome were annotated with
531 RepeatMasker[53] version 4.1.1 with the -cutoff 250, -nolow, -no_is, and -norna options to identify their
532 locations in the *M. oryzae* Guy11 genome. For read coverage plots as well as histone and GC content
533 plots, full length LTR retrotransposon copies were required. These were identified by using the original
534 full length consensus sequences with RepeatMasker as before and then filtered to hits greater than
535 3000 bp in length and greater than 90% sequence identity.

536 **Comparative analysis of eccDNA forming regions**

537 Analysis of eccDNA forming regions in organisms other than *M. oryzae* were performed as described
538 above for Illumina sequencing data using previously published genome, gene annotation and
539 transposable element annotation files (Supplemental Data File 30). However, unlike the other data used
540 in this study, the sequencing data in the *S. cerevisiae* dataset was single-end and therefore opposite
541 facing read pairs could not be used to infer eccDNA forming regions. Instead, only eccDNA forming
542 regions with three overlapping junction split reads were used for analysis. For all organisms, reads
543 mapping to unplaced scaffolds and organellar genomes were removed after mapping as described
544 above for the *M. oryzae* mitochondrial genome. These scaffolds were also removed from genome size,
545 number of coding base pairs, and number of LTR retrotransposon base pairs calculations for
546 comparative analysis.

547 **Characterization of eccDNA formation by LTR retrotransposons**

548 To generate the Manhattan plot, junction split reads were filtered by selecting regions that were made
549 up of 90% LTR retrotransposon sequences. Junction split read coverage was then calculated for each 100
550 bp window in the genome. Coverage values were then normalized to the total number of LTR eccDNA
551 junction split reads per sample. These coverage values were then averaged across technical replicates
552 for each biological replicate, and then averaged across biological replicates. Finally, only 100 bp bins that
553 overlapped at least 50 bp with an LTR retrotransposon were plotted.

554 To simulate expected read coverage for different types of LTR eccDNAs, the Copia1 consensus sequence
555 was taken as a reference, though other consensus sequences yielded identical results. Simulated DNA
556 sequences were then generated for each type of LTR eccDNA. The expected 2-LTR circular sequence
557 generated by NHEJ (scenario 1, Figure 3A) was simply made up of two LTR sequences and the internal
558 sequence, and the expected 1-LTR circle sequence generated by HR (scenario 3, Figure 3C) was made up
559 of one LTR sequence and the internal sequence. These sequences were shuffled 1000 times to generate
560 1000 sequences starting at various points of the expected circularized sequence. For the 1-LTR circle
561 sequence generated by autointegration (scenario 2, Figure 3B), the random autointegration events were
562 simulated by choosing a random length segment of the internal sequence starting with its start or end,
563 adding the LTR sequence to this sequence, and randomly shuffling the sequence to simulate a circular
564 sequence. This process was repeated 1000 times to generate 1000 sequences. Finally, for each scenario,
565 Illumina reads were simulated to reach 2000x coverage for each of the simulated sequences using ART
566 Illumina[54] version 4.5.8 and the following parameters: 150 bp read length, 450 bp mean insert size, 50
567 bp insert size standard deviation, HiSeqX TruSeq. Reads were mapped to the simulated sequences using
568 BWA-MEM[45] version 0.7.17-r1188 with default settings and coverage for each base pair was calculated.

569 To generate observed coverage for each element, sequencing read coverage across the genome was
570 calculated for all 10 base pair windows in the *M. oryzae* Guy11 genome for each sample. Coverage
571 values were then normalized to the total number of mapped sequencing reads in each sample. These
572 coverage values were then averaged across technical replicates for each biological replicate, and then
573 averaged across biological replicates. Finally, profile plot data was generated for full length, high
574 confidence sequences for each LTR retrotransposon using computeMatrix scale-regions and plotProfile
575 of the DeepTools[55] suite of tools version 3.5.1 using full length, high confidence LTR retrotransposon
576 sequences.

577 **Identification of split reads associated with eccDNA formation from LTR retrotransposons**

578 Split reads were first identified as any read that mapped to only two places in the genome with at least
579 20 base pairs of alignment on either side. LTR-LTR split reads were then selected from these split reads
580 for each LTR retrotransposon if both sides of the split read had any overlap with any copy of that
581 retrotransposon's LTR in the genome. LTR-internal split reads were selected if one side of the split read
582 had any overlap with any copy of the retrotransposon's LTR in the genome and the other side had any
583 overlap with any copy of the retrotransposon's internal region in the genome. Read coverage, LTR-LTR
584 split read coverage, and LTR-internal coverage was then calculated for each annotation of each LTR
585 retrotransposon. Coverage values were then normalized to the total number of mapped sequencing
586 reads in each sample. These coverage values were then averaged across technical replicates for each
587 biological replicate, and then averaged across biological replicates.

588 **Analysis of eccDNA formation from specific genomic regions**

589 Genome, gene annotation, and transposable element annotation files for each organism used for this
590 analysis were as previously described (Supplemental Data File 30). Again, organellar genomes as well as
591 unplaced contigs were filtered out of these files before analysis. Introns and UTRs were added to gene
592 annotation files that were missing these elements using the 'agat_convert_sp_gff2gtf.pl' and
593 'agat_sp_add_introns.pl' commands from the AGAT toolkit version 0.6.2
594 (https://github.com/NBISweden/AGAT). Cpgplot of EMBOSS[56] version 6.6.0.0 was used to annotate CpG
595 islands in each genome. Upstream and downstream regions were defined as being 2000 base pairs
596 upstream from the transcription start site and downstream from the transcription end site, respectively.
597 Genic regions were defined as being made up of all sequences between transcription start and end sites
598 and intergenic regions were the opposite. Junction split reads were counted as being from a specific
599 region if they overlapped to any extent within that region.

600 The observed percentage of junction split reads overlapping with each region type was calculated for
601 each sample for each organism and an average of these percentages was calculated. The junction split
602 reads of each sample were then shuffled across the genome 10 times, excluding LTR retrotransposon
603 locations, and an expected percentage for each region was calculated, averaged across all permutations,
604 then averaged across all samples for each organism. Finally, the log 2 fold enrichment was calculated by
605 taking the log 2 of the observed average percentage over the expected average percentage.

606 **Expression and junction split read counts per gene**

607 Previously published RNAseq data from *M. oryzae* Guy11 grown in liquid culture in rich medium was
608 obtained[57] (Supplemental Data File 31). The data was mapped to the *M. oryzae* Guy11 genome using
609 STAR[58] version 2.7.1a with the quantMode GeneCounts option. Read counts per gene were then divided
610 by library size and multiplied by the length of each gene in order to obtain reads per kilobase million
611 (RPKMs). RPKMs per gene were then averaged across all samples.

612 Junction split read counts per gene used to analyze the correlation of expression and eccDNA formation
613 were generated for each gene by counting the number of junction split reads that intersect the gene to
614 any extent. Counts per gene were first assessed for each technical replicate and normalized to the
615 number of junction split reads in that sample. Normalized counts were then averaged across technical

616 replicates for each biological replicate. Average counts per biological replicate were then averaged to
617 obtain the final result.

618 **Genes and junction split read counts per 100kbp**

619 The *M. oryzae* genome was divided into 100kbp bins and the number of genes per bin was then
620 calculated. Junction split reads per bin were calculated for each sample using the same method.
621 Junction split read per bin values were then normalized to the total number of junction split reads in
622 each sample. These values were then averaged across technical replicates for each biological replicate,
623 and then averaged across biological replicates.

624 **ACS enrichment analysis**

625 The published ACS sequence profile[35] was used to identify ACSs in eccDNA forming regions using the
626 FIMO[59] software version 4.12.0. Only hits scoring greater than 17 were kept. In order to test for
627 enrichment of these sequences, an expected distribution of ACS sequences was generated by randomly
628 shuffling eccDNA forming regions across the *M. oryzae* Guy11 genome, excluding regions containing LTR
629 retrotransposons. The observed number of ACS sequences in eccDNA forming regions was then
630 compared to the expected distribution to generate a p-value.

631 **Histone mark and GC content profile plots**

632 Previously published ChIPSeq data for H3K27me3, H3K27ac, H3K36me3 and loading controls was
633 obtained[57]. Sequencing reads for each technical replicate were combined before reads for each
634 treatment for each biological replicate were mapped to the *M. oryzae* Guy11 genome using BWA-MEM[45]
635 version 0.7.17-r1188 with default settings. The bamCompare command from the DeepTools[55] suite of
636 tools version 3.5.1 with the scaleFactorsMethod readCount option was then used to compare the signal
637 from each treatment to the loading control for each biological replicate. computeMatrix scale-regions
638 was then used in conjunction with the plotProfile command to generate processed data for profile plots.
639 After verifying that all biological replicates resulted in similar profile plots, only the first biological
640 replicate was chosen for presentation.

641 To generate tracks used for profile plots, a few different strategies were used. GC content profile plots
642 by calculating GC percentage for 50 base pair windows throughout the genome. Profile plot data was
643 then generated using computeMatrix scale-regions and plotProfile commands as before. Methylated
644 and acetylated genes were determined using the methylation and acetylation peaks published by Zhang
645 *et al*[57]. Marked genes were called when at least 50% of the gene overlapped with a peak. Large
646 eccDNAs, microDNAs, and LTR-eccDNAs from all *M. oryzae* Guy11 samples were combined into a single
647 list which was filtered for duplicates and used for the corresponding tracks in the profile plots. The
648 genome baseline track was generated by combining all of these eccDNA forming regions and shuffling
649 them randomly across the genome. Finally, the full length, high quality LTR-retrotransposon annotations
650 described above were used for LTR retrotransposon tracks. The same approach was used for generating
651 profile plots to compare histone marks and GC content for eccDNA-associated and eccDNA-absent
652 genes.

653 **Encompassing split read counts per gene**

654 Encompassing split read counts per gene for determining eccDNA-associated and eccDNA-absent genes
655 were generated for each gene by counting the junction split reads that fully encompass the gene using
656 the intersect command of the BEDTools[60] suite version 2.28.0 with the -f 1 option. This count was
657 normalized to the total number of junction split reads in each sample, then averaged across technical
658 replicates for each biological replicate, then averaged across biological replicates to obtain the final
659 encompassing split read count per gene.

660 **GO enrichment analysis**

661 GO terms were first assigned to annotated *M. oryzae* Guy11 genes using the PANNZER2[61] webserver on
662 August 17th, 2020. The topGO[62] R package version 2.36.0 was then used to parse assigned GO terms and
663 reduce the gene list to a list of feasible genes for analysis. Either eccDNA-associated or eccDNA-absent
664 were assigned as significant genes, and the number of these genes belonging to each GO term was used
665 as the observed value for the enrichment analysis. A kernel density function was then generated using
666 the gene lengths of the significant gene set. The same number of genes as the significant gene set were
667 then sampled at random from the feasible gene set using weighted random selection with weights
668 obtained from the kernel density function. This random sampling was repeated 100 times and the
669 average of the number of genes belonging to each GO term was used as the expected value for the
670 enrichment analysis. Finally, the chi-square statistic was then computed comparing observed and
671 expected values to test for enrichment or depletion of each GO term.

672 **Gene presence absence variation**

673 In order to identify genes prone to presence absence variation in the *M. oryzae* Guy11 genome,
674 OrthoFinder[63] version 2.5.1 with default settings was used on all of the *M. oryzae* proteomes and the
675 *Neurospora crassa* proteome obtained from GenBank (accession GCA_000182925.2). Then, for each *M.*
676 *oryzae* genome, we queried whether each gene annotated in the *M. oryzae* Guy11 genome had an
677 ortholog identified by OrthoFinder in that genome. Finally, the absence of genes without orthologues
678 was confirmed using BLASTN[50] version 2.7.1+.

679 **Effector annotation**

680 Effectors were predicted among *M. oryzae* Guy11 genes by first selecting genes with signal peptides
681 which were predicted using SignalP[64] version 5.0b Darwin x86_64. Genes with predicted transmembrane
682 domains from TMHMM[65] version 2.0c were then excluded. Finally, EffectorP[66] version 2.0 was used to
683 predict effectors from this secreted gene set. Previously well-characterized effectors were identified
684 using previously published protein sequences[38] and DIAMOND[67] version 2.0.9.147.

685 **Identification of small, genic deletions**

686 Small, genic deletions were identified using orthologs identified by OrthoFinder[63] version 2.5.1 as
687 before. For each genome, we looked for genes in the *M. oryzae* Guy11 genome that had no ortholog in
688 that genome, but that were flanked by two genes with orthologs in that genome. One-to-many, many-
689 to-many, and many-to-one orthologs were excluded from this analysis. Candidate gene deletions were
690 validated using alignments performed using the nucmer and mummerplot commands of the MUMmer[68]
691 suite of tools version 4.0.0rc1 to verify that a DNA deletion truly existed, and that this deletion
692 overlapped the gene of interest.

693 **Identification of eccDNA-mediated translocations**

694 Identification of translocations with a potential eccDNA intermediate was done by first aligning two
695 genomes using the nucmer command of the MUMmer[68] suite of tools version 4.0.0rc1 with the
696 maxmatch option. The nucmer output was then parsed to look for portions of the reference genome
697 that had an upstream region that aligned to one query scaffold, followed by two separate adjacent
698 alignments to another query scaffold, followed by a downstream region that aligned to the original
699 query scaffold. We also required that the two adjacent alignments in the center of the region were to
700 adjacent regions in the query scaffold but their order was reversed compared to the reference.
701 Candidate eccDNA-mediated translocations were verified manually by inspecting alignment plots
702 generated using the mummerplot command. The *S. cerevisiae* EC1118 (GCA_000218975.1) and M22
703 genomes (GCA_000182075.2) obtained from GenBank were used to verify the ability of our pipeline to
704 detect these translocation events. The *M. oryzae* Guy11 genome was then compared to 306 *M. oryzae*
705 genomes (Supplemental Data File 25) to look for these events in the *M. oryzae* species. Before
706 alignment, transposable elements were masked from these *M. oryzae* genomes using RepeatMasker[53]
707 version 4.1.1 with the -cutoff 250, -nolow, -no_is, and -norna options, as well as a transposable
708 elements library generated by combining the RepBase[48] fngrep version 25.10 with the de novo repeat
709 library generated by RepeatModeler[49] version 2.0.1 run on the *M. oryzae* Guy11 genome with default
710 settings aside from the -LTRStuct argument.

711 **Minichromosome genes and eccDNAs**

712 Scaffolds corresponding to minichromosomes in the *M. oryzae* FR13 (GCA_900474655.3), CD156
713 (GCA_900474475.3), and US71 (GCA_900474175.3) genomes were extracted according to previously
714 published information[69]. Exonerate[70] version 2.4.0 was then used with the protein2genome model to
715 identify genes in the *M. oryzae* Guy11 genome that were found on minichromosomes in these other
716 isolates. Hits with greater than 70% sequence identity to any minichromosome scaffold were identified
717 as genes found on minichromosomes. Encompassing split reads were then counted for all genes. This
718 count was normalized to total number of junction split reads in each sample, then averaged across
719 technical replicates for each biological replicate, then averaged across biological replicates. Finally,
720 normalized encompassing split read counts for genes found on minichromosomes were compared to
721 genes not found on minichromosomes.

722 **Rarefaction analysis**

723 Rarefaction analysis for genes found fully encompassed by eccDNA forming regions were performed by
724 first sampling eccDNA forming regions from all samples at random in increasing 10% intervals. For each
725 subsample, the number of genes found fully encompassed by eccDNA forming regions was determined
726 as before. Next, eccDNA forming regions were shuffled across the genome and sampled at random in
727 increasing 10% intervals. Again, the number of genes found fully encompassed by eccDNA forming
728 regions was determined for each sample. This analysis was performed 100 times with similar results as
729 those represented in Figure 5C. A similar approach was used for rarefaction analysis of eccDNA forming
730 regions but the number of unique microDNAs, large eccDNAs and LTR-eccDNAs were counted at each
731 subsample instead.

732 **Code and Code availability**

Data processing was performed in a RedHat Enterprise Linux environment with GNU bash version 4.2.46(20)-release. GNU coreutils version 8.22, GNU grep version 2.20, GNU sed version 4.2.2, gzip version 1.5, and GNU awk version 4.0.2 were all used for file processing and handling. Conda version 4.8.2 (https://docs.conda.io/en/latest/) was used to facilitate installation of software and packages. Code parallelization was performed with GNU parallel[71] version 20180322. Previously published data was downloaded using curl version 7.65.3 (https://curl.se/) and sra-tools version 2.10.4 (https://github.com/ncbi/sra-tools). Image file processing was performed with the help of ghostscript version 9.25 (https://ghostscript.com/) and imagemagick version 7.0.4-7 (https://imagemagick.org/index.php). BED format files were processed using bedtools[60] version 2.28.0 and bedGraphToBigWig version 4 (https://www.encodeproject.org/software/bedgraphtobigwig/). SAM and BAM format files were processed with SAMtools[72] version 1.8 and Picard version 2.9.0 (https://broadinstitute.github.io/picard/).

Data processing was also facilitated by custom Python scripts written in Python version 3.7.4 with the help of the pandas[73] version 0.25.1 and numpy[74] version 1.17.2 modules. The scipy[75] version 1.4.1 and more-intertools version 7.2.0 (https://more-itertools.readthedocs.io/) modules were also used.

Data analysis and statistical analyses were performed in R version 3.6.1. Data handling was processed using data.table[76] version 1.13.6, tidyr[77] version 1.1.3, reshape2[78] version 1.4.4, and dplyr[79] version 1.0.4 packages. Plotting was performed using the ggplot2[80] version 3.3.5 package, with help from RColorBrewer[81] version 1.1.2, scales[82] version 1.1.1, cowplot[83] version 1.1.1, ggprepel[84] version 0.9.1 and ggpubr[85] version 0.4.0 packages. The Gviz[86] version 1.28.3 was used for BAM file visualization. Supplemental tables were made using gt[87] version 0.3.1.

Code for the pipeline used to call eccDNA forming regions for Illumina sequencing data is available in this maintained GitHub repository: https://github.com/pierrj/ecc_caller

All other code used for raw data processing, data analysis, and figure generation is available in this GitHub repository: https://github.com/pierrj/moryzae_eccdnas_manuscript_analysis_and_plots

Data availability

All data in this study has been submitted to NCBI's Sequence Read Archive and Zenodo. Illumina circularome sequencing data for *M. oryzae* was submitted under BioProject accession PRJNA768097. PacBio circularome sequencing data for *M. oryzae* was submitted under BioProject accession PRJNA556909. Illumina circularome sequencing data for *O. sativa* was submitted under BioProject accession PRJNA768410.

Genomes and annotation files used for comparative circularome analysis are available here:

https://zenodo.org/record/5544950#.YVtyHe3MKUk

Annotated genes and predicted proteins for rice-infecting *M. oryzae* isolates are available here:

https://zenodo.org/record/5542597#.YVtxvO3MKUk

Output from OrthoFinder2 run on rice-infecting *M. oryzae* proteomes is available here:

https://zenodo.org/record/5544260#.YVtyWe3MKUk

All files used for statistical analysis and plotting are available here:

https://zenodo.org/record/5565321#.YWXknGLMKUk

Acknowledgements

We thank Snighda Poddar for providing the *M. oryzae* Guy11 isolate and for advice for culturing the pathogen. We thank Ursula Oggenfuss for advice on using WICKERsoft for generating LTR retrotransposon consensus sequences. We also thank the Krasileva lab for feedback on manuscript preparation. This research used the Savio computational cluster resource provided by the Berkeley Research Computing program at the University of California, Berkeley (supported by the UC Berkeley Chancellor, Vice Chancellor for Research, and Chief Information Officer). We also thank Novogene (Tianjin, China) for technical support. Pierre M. Joubert has been supported by the Grace Kase graduate fellowship and Ksenia V. Krasileva has been supported by funding from Innovative Genomics Institute as well as the Gordon and Betty Moore Foundation (8802).

783 **Figures**

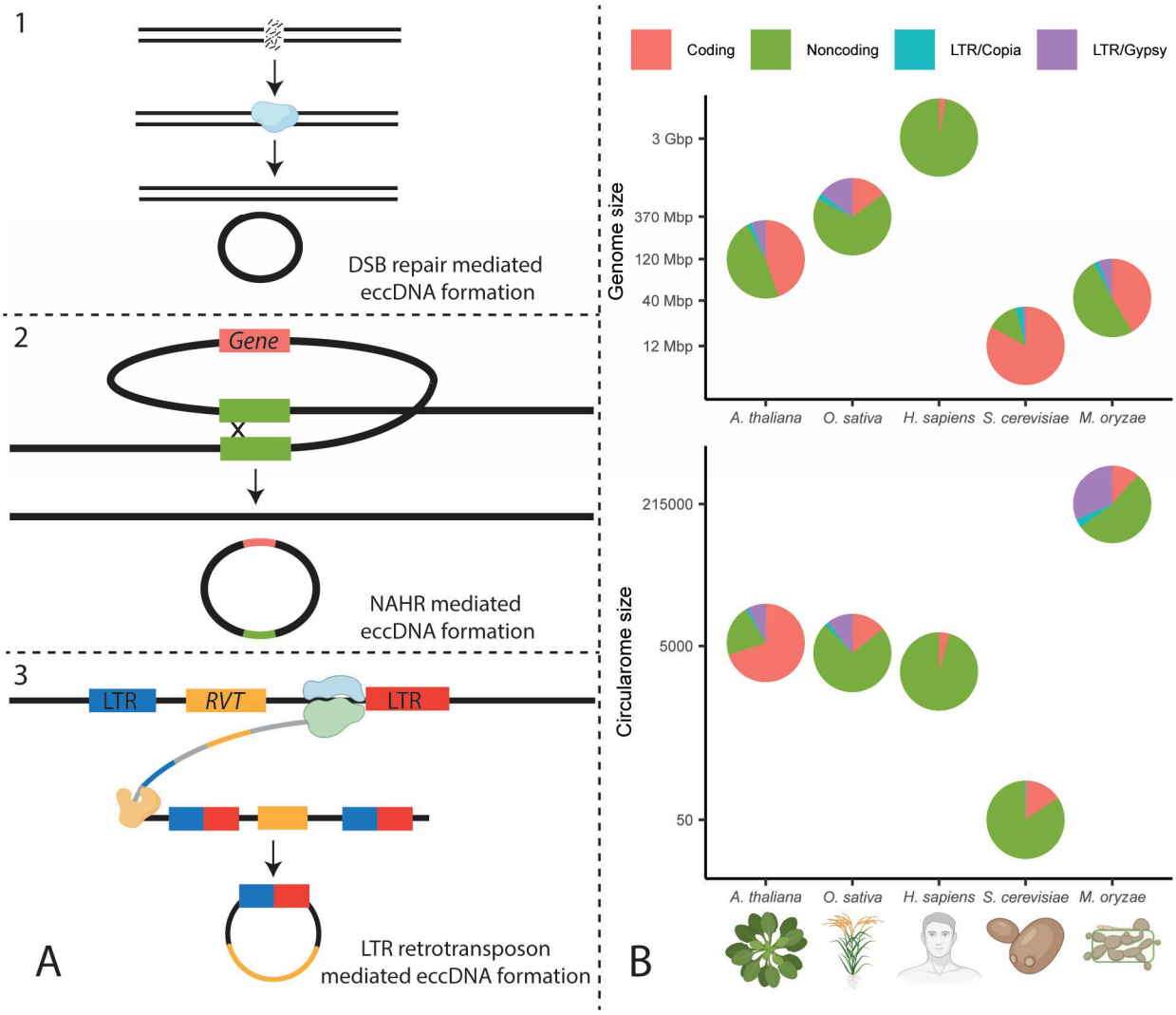

784

785 **Figure 1.** A. Examples of mechanisms of extrachromosomal circular DNA (eccDNA) formation. 1. eccDNA
786 formation as a result of double strand break repair. The blue enzyme represents several different types
787 of DNA repair mechanisms 2. eccDNA formation as a result of nonallelic homologous recombination
788 (NAHR). The green boxes represent homologous sequences. 3. eccDNA formation as a result of LTR
789 retrotransposon activity. The blue and green enzyme represents the ribosome, and the orange enzyme
790 represents a reverse transcriptase (RVT). Rectangles that are partly blue and partly red represent hybrid
791 LTRs formed from 5' and 3' LTRs during retrotransposition. DNA is drawn in black and RNA in gray. B.
792 Comparison of genome size and circularome size for *Arabidopsis thaliana*, *Oryza sativa*, *Homo sapiens*,
793 *Saccharomyces cerevisiae* and *Magnaporthe oryzae.* Circularome size is shown as the number of eccDNA
794 forming regions called by our pipeline in an average sample. Only circularome data for *A. thaliana* and
795 *O. sativa* leaf tissue, *H. sapiens* muscle tissue, and *S. cerevisiae* deletion collection samples are shown.
796 Additionally, only *A. thaliana* circularome data from Wang et al. 2021 and *O. sativa* data from Lanciano
797 et al. 2017 are shown. The organism icons were created with BioRender.com.

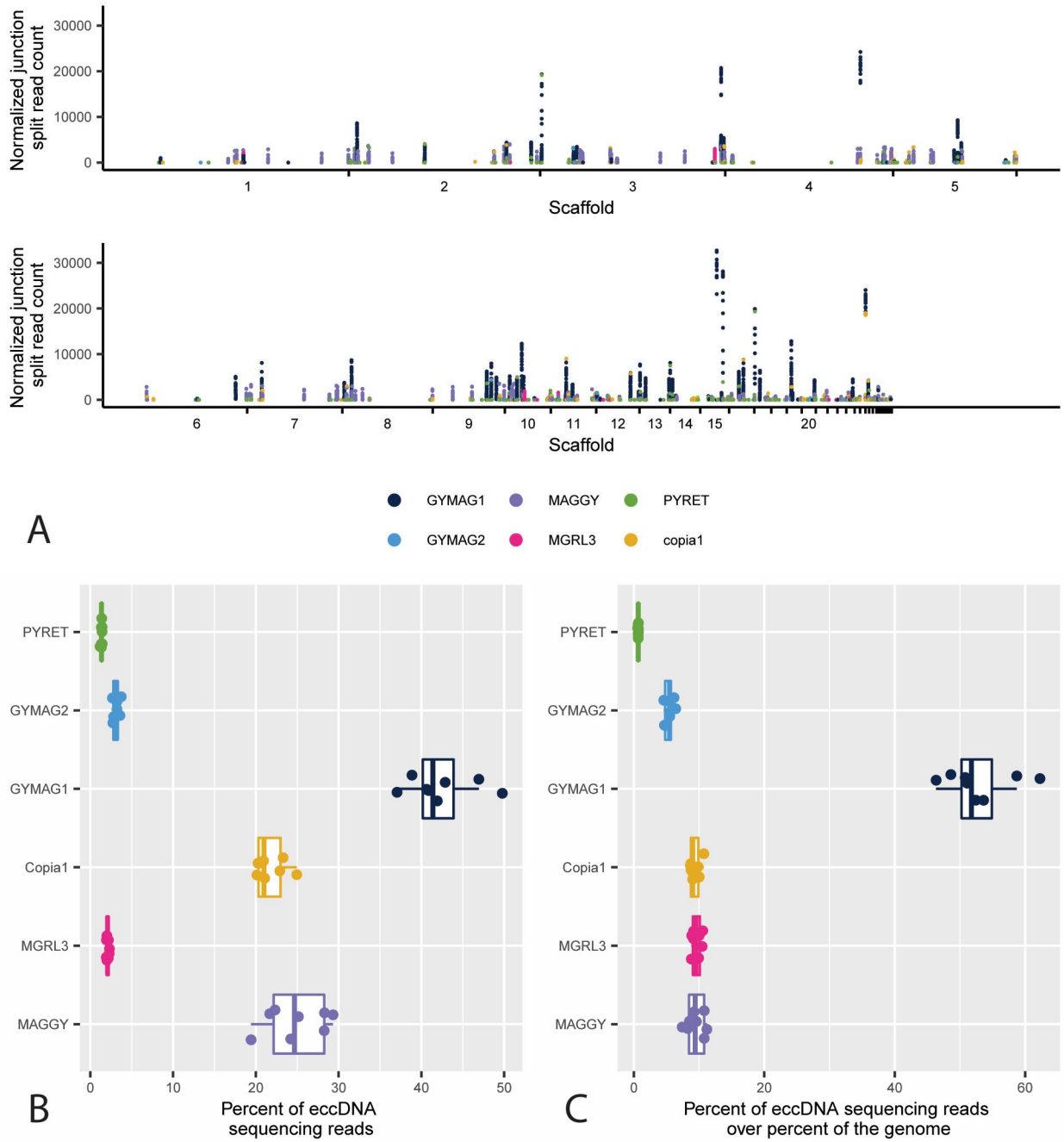

Figure 2. A. Manhattan plot showing the number of junction split reads per million averaged across all sequenced samples for all 100 bp bins that overlap an LTR retrotransposon. Each dot represents one of these bins. B. Boxplot showing the percentage of sequencing reads that map to LTR retrotransposons. Each dot represents one sequenced sample. C. Boxplot showing the ratio of the percentage of sequencing reads that map to LTR retrotransposons to the percentage of the *M. oryzae* Guy11 genome that is made up by that retrotransposon. Each dot represents one sequenced sample.

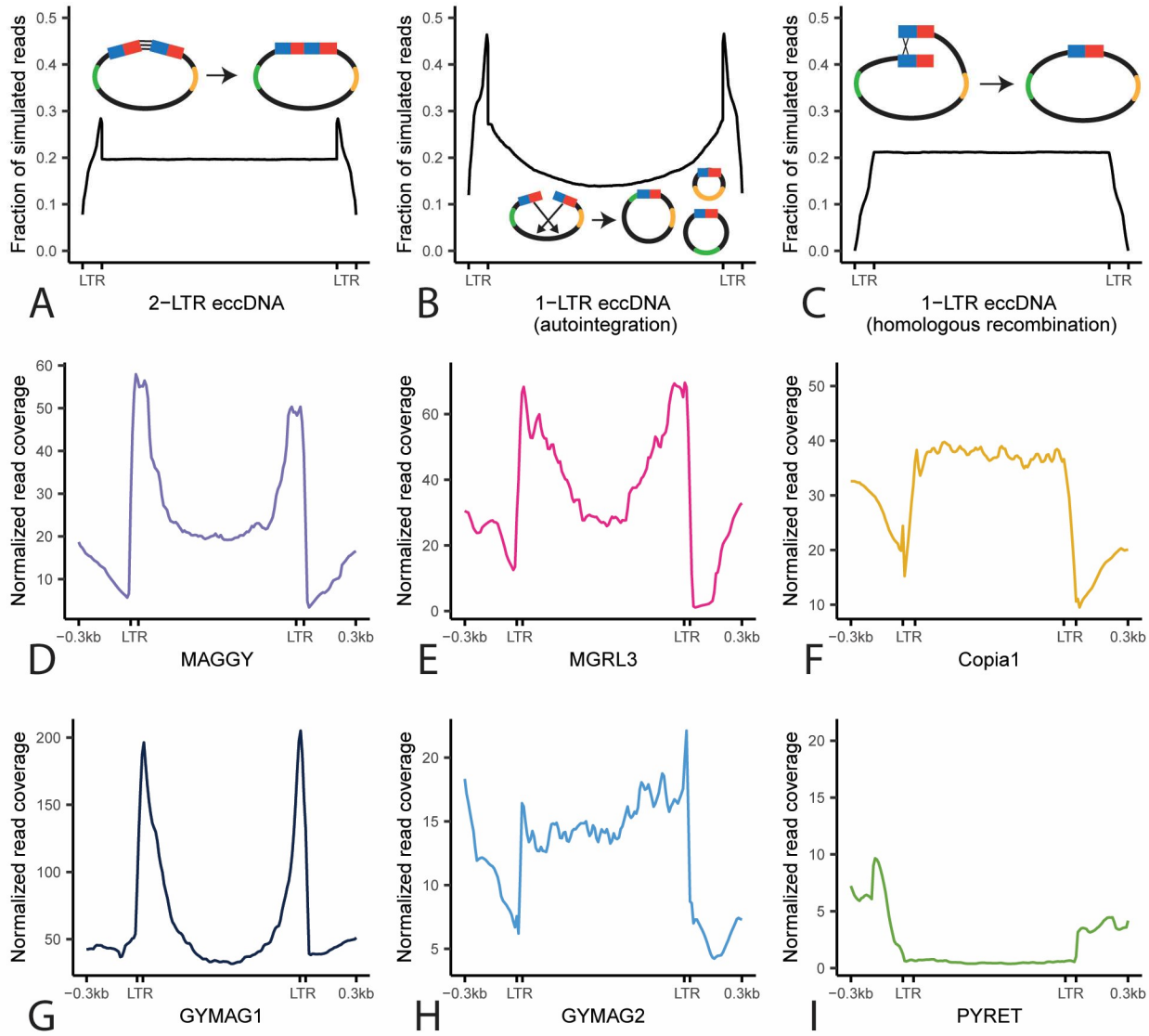

Figure 3. A-C. Profile plots showing expected sequencing read coverage for each LTR retrotransposon eccDNA formation scenario as well as graphical representations of the scenario. In the graphics, blue and red rectangles represent hybrid LTRs formed from 5' and 3' LTRs during retrotransposition and green and orange represent areas of the internal region of the retrotransposon with distinct sequences. D-I. Profile plots showing observed sequencing read coverage for each LTR retrotransposon found in the *M. oryzae* Guy11 genome.

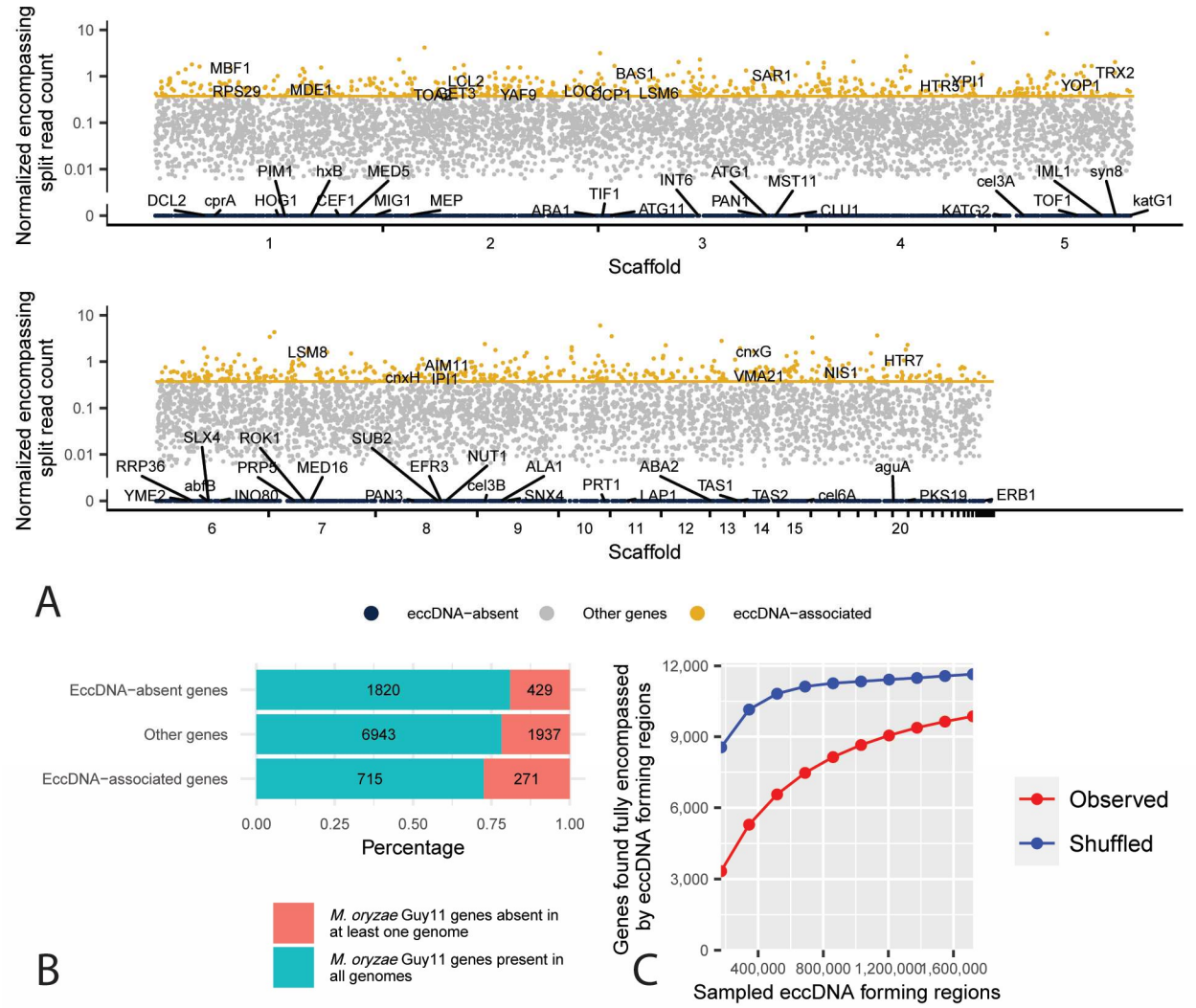

Figure 4. A. Manhattan plot showing the number of encompassing split reads per million junction split reads averaged across all sequenced samples for each gene in the *M. oryzae* Guy11 genome. Each dot represents one gene. The orange line represents the cutoff between eccDNA-associated genes and other genes. EccDNA-associated genes with known gene names are labeled according to their normalized encompassing split read count and position in the genome. EccDNA-absent genes with known gene names are labeled with lines pointing to their location in the genome. B. Stacked bar plot showing the percentage of eccDNA-absent genes, other genes, and eccDNA-associated genes in the *M. oryzae* Guy11 genome that had an ortholog in all other 162 *M. oryzae* genomes analyzed or not. Numbers indicate the number of genes in each category. C. Rarefaction analysis of the observed number of genes found fully encompassed by eccDNA forming regions at different subsamples of all found eccDNA forming regions, compared to the same number of randomly selected genomic regions.

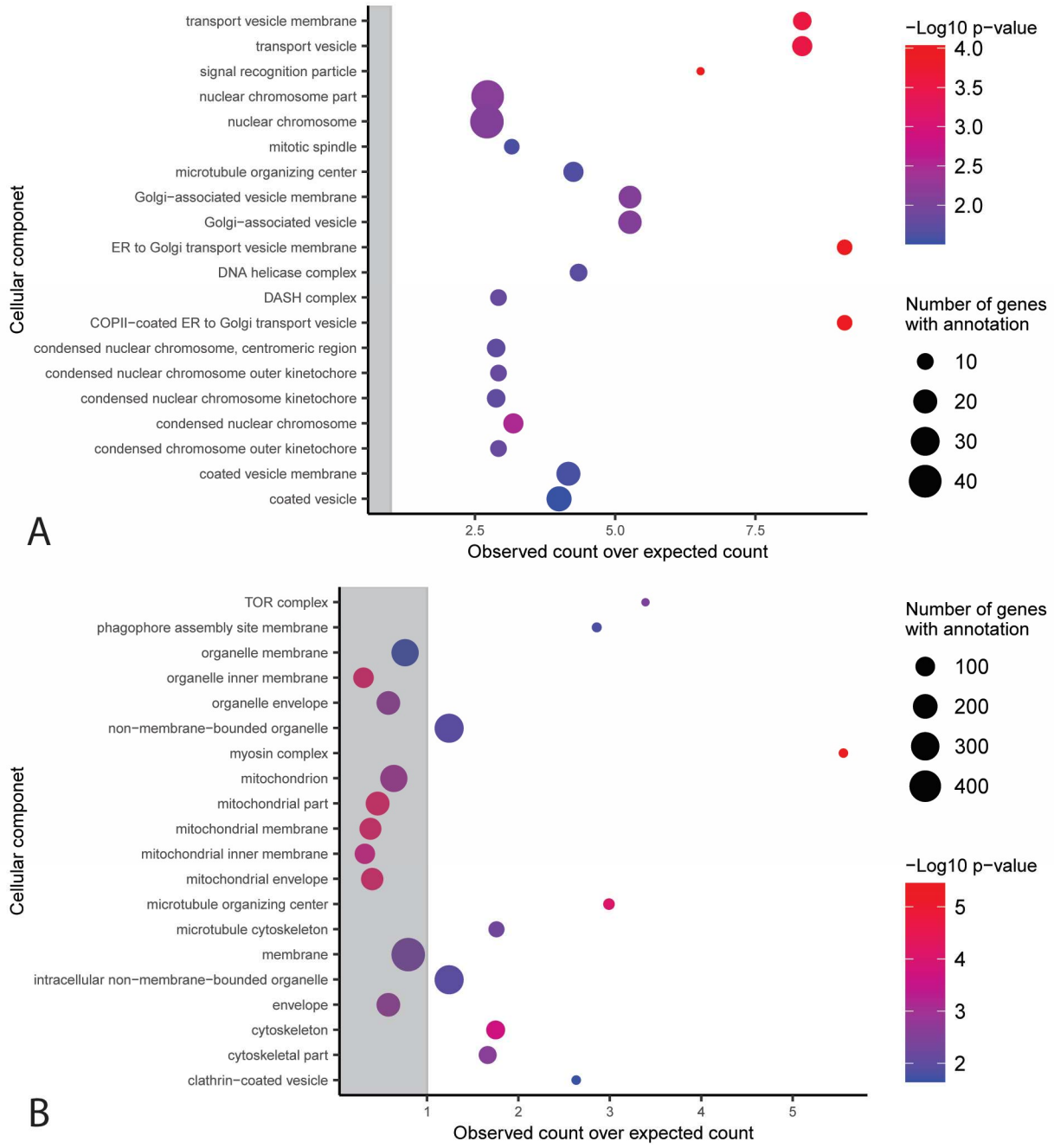

Figure 5. Functional categories in the cellular component Gene Ontology with an observed number of A. eccDNA-associated genes or B. eccDNA-absent genes that is significantly different from the expected number with correction for gene length bias (Chi-square test, $p < 0.05$). The y-axis shows the different functional categories, and the x-axis represents the observed number of genes divided by the expected number of genes in this group. Dots outside of the grey rectangle represent functional categories that are observed more often than expected. The size of dots indicates the total number of genes in the *M. oryzae* genome that belong to each functional category. Only the 20 categories with the largest -log10 p-values are shown.

834

835

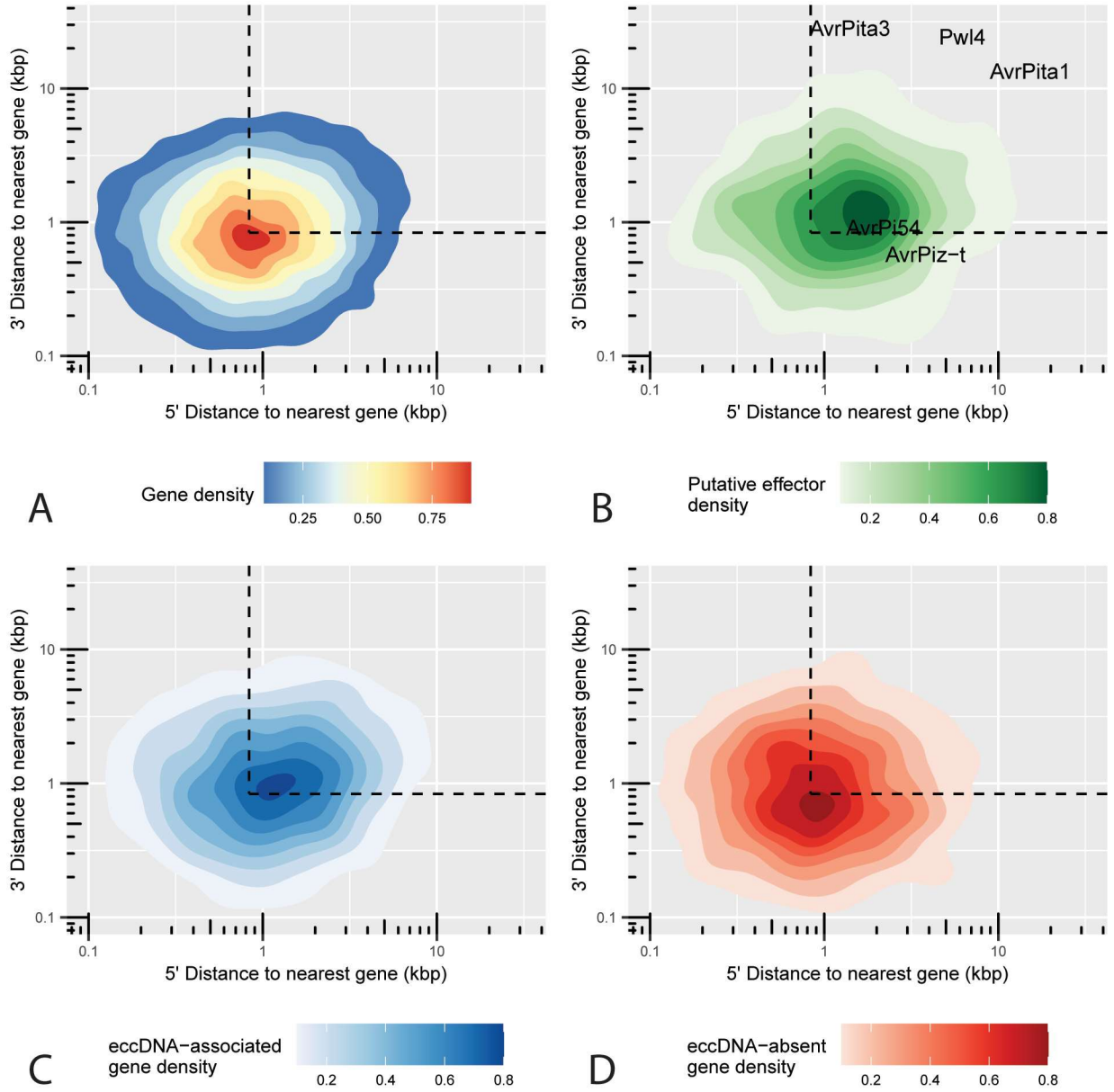

836

837 **Figure 6.** Two-dimensional density plot representing the 5' and 3' distance to the nearest gene in the *M.*
838 *oryzae* Guy11 genome in kilobase pairs for each A. gene, B. predicted effector, C. eccDNA-associated
839 genes, and D. eccDNA-absent genes. Known effectors are shown as text in B. Dashed lines represent
840 median 5' and 3' distance to nearest gene.

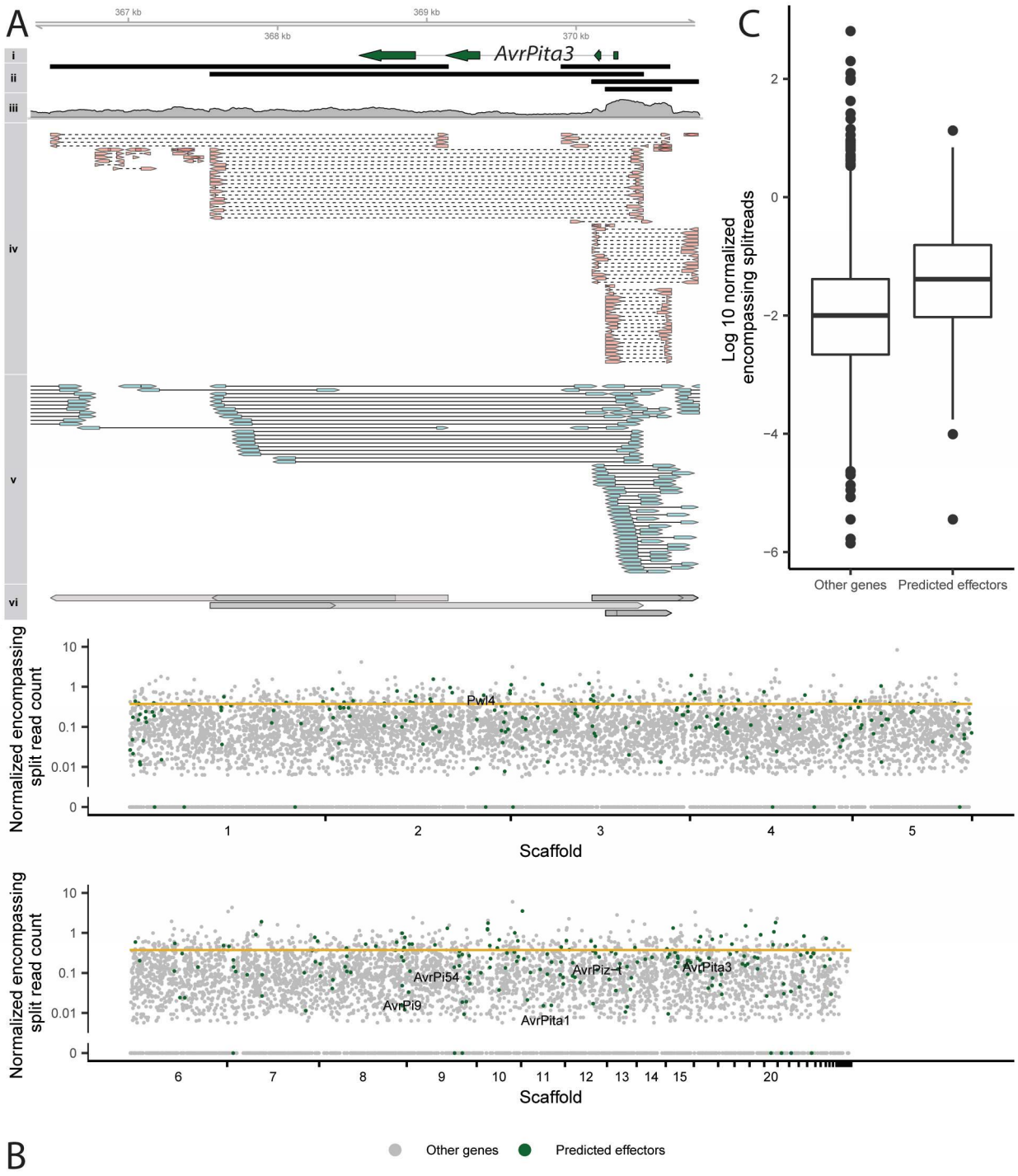

Figure 7. A. Example of an effector found on an eccDNA. i. location of effector *AvrPita3*. ii. Location of eccDNA forming regions. iii. Overall sequencing read coverage. iv. Junction split reads. Split reads are joined by a dashed line. v. Opposite facing read pairs. Read pairs are joined by a solid line. vi. PacBio split reads. Overlaps are from single reads mapped to the same location more than once. All data was obtained from a single sequenced sample. B. Manhattan plot showing the number of encompassing split reads per million averaged across all sequenced samples for each gene in the *M. oryzae* Guy11 genome.

848 Each dot represents one gene. The orange line represents the cutoff for eccDNA-associated genes.
849 Known effectors are shown as text. C. Box plot showing the log 10 of the number of fully encompassing
850 junction split reads per million junction split reads averaged across all sequenced samples for predicted
851 effectors compared to all other genes.

852

853 **Supplemental Figures**

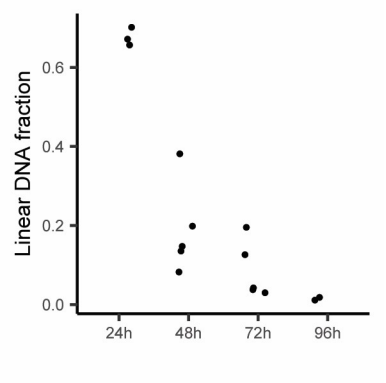

854

855 **Supplemental Figure 1.** Scatter plot showing the effect of exonuclease treatment on linear DNA fraction
856 of total extracted DNA from *M. oryzae* tissue samples. Each dot represents one biological replicate
857 averaged across four technical replicates.

858

859

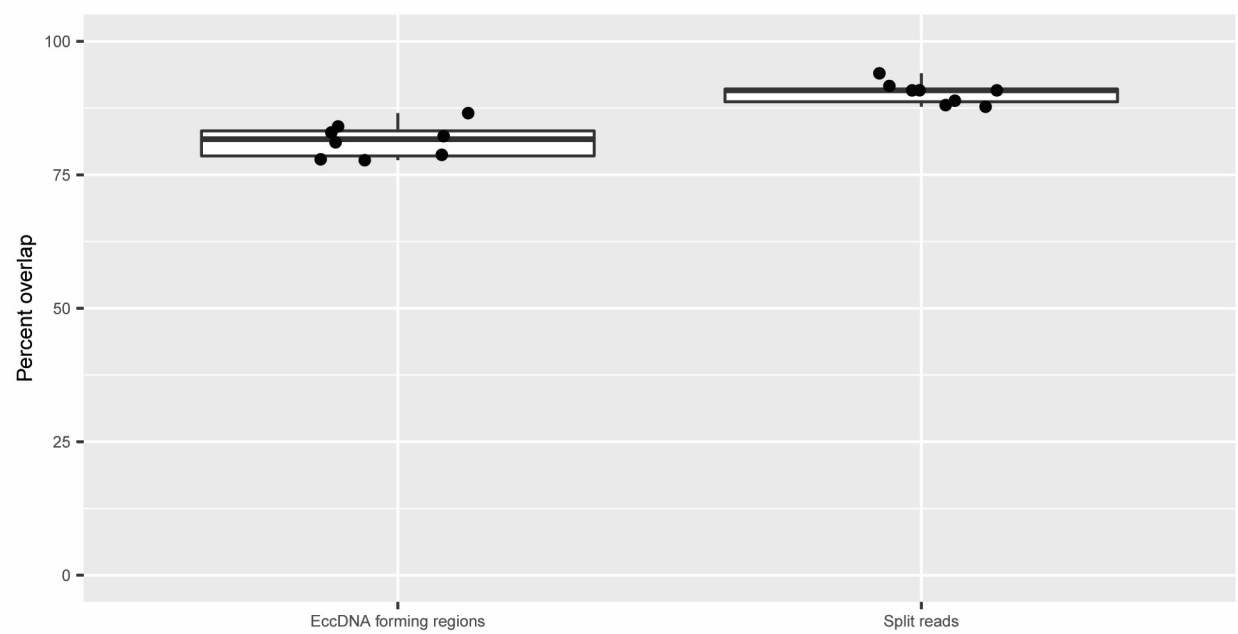

860

861 **Supplemental Figure 2.** Boxplot showing the percentage of eccDNA forming regions that were found in
862 each sample using our PacBio sequencing data that were also represented in either eccDNA forming
863 regions called using our Illumina sequencing data or split reads found in this data. Each point represents
864 one sample.

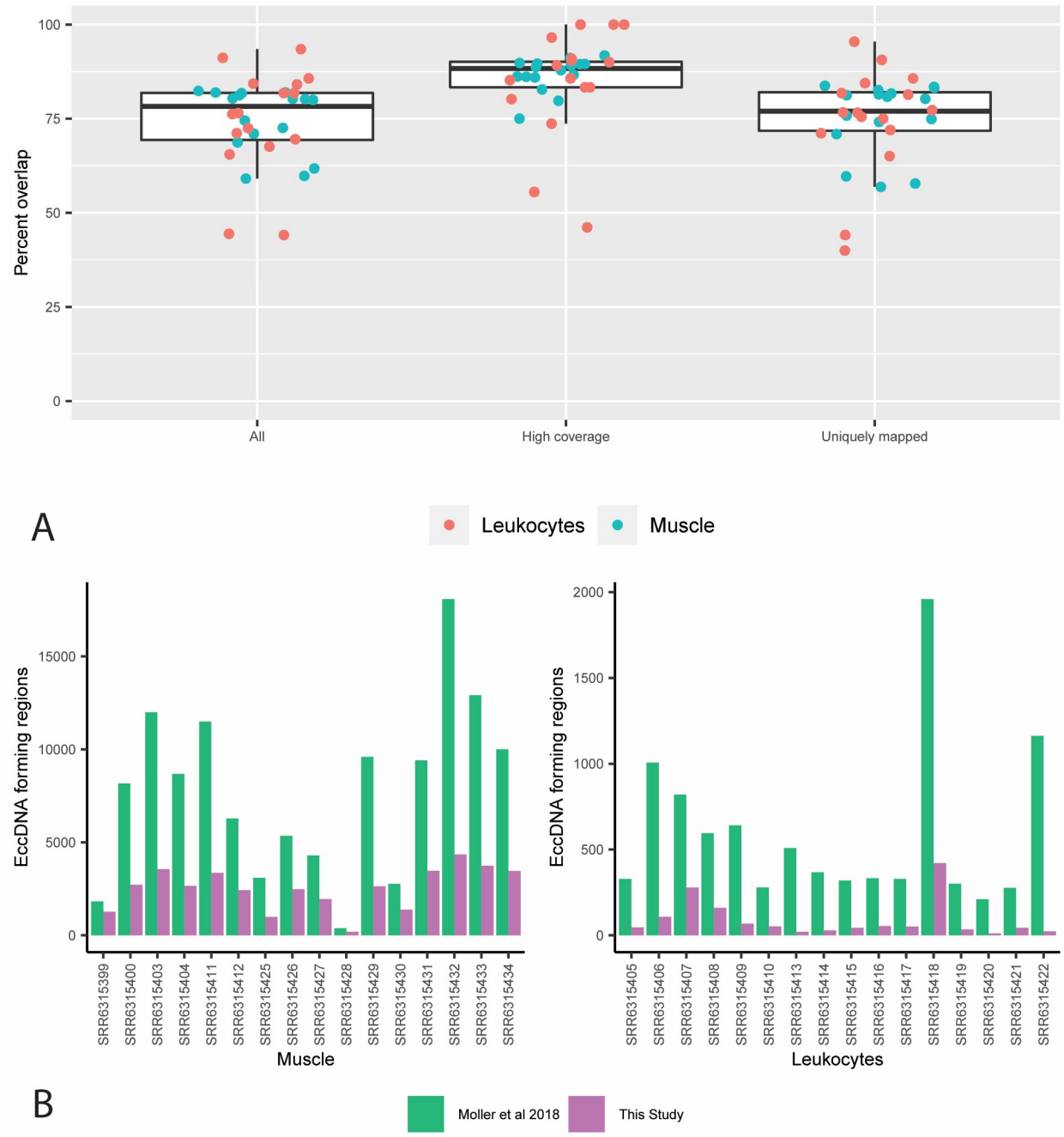

Supplemental Figure 3. A. Boxplot showing the percentage of eccDNA forming regions that were found using our pipeline that were also found in the published eccDNA forming regions for human samples. Each dot represents one sample. B. Bar plot showing counts of eccDNA forming regions generated from our pipeline compared to counts in published data. Sample IDs are from the Sequence Read Archive (SRA).

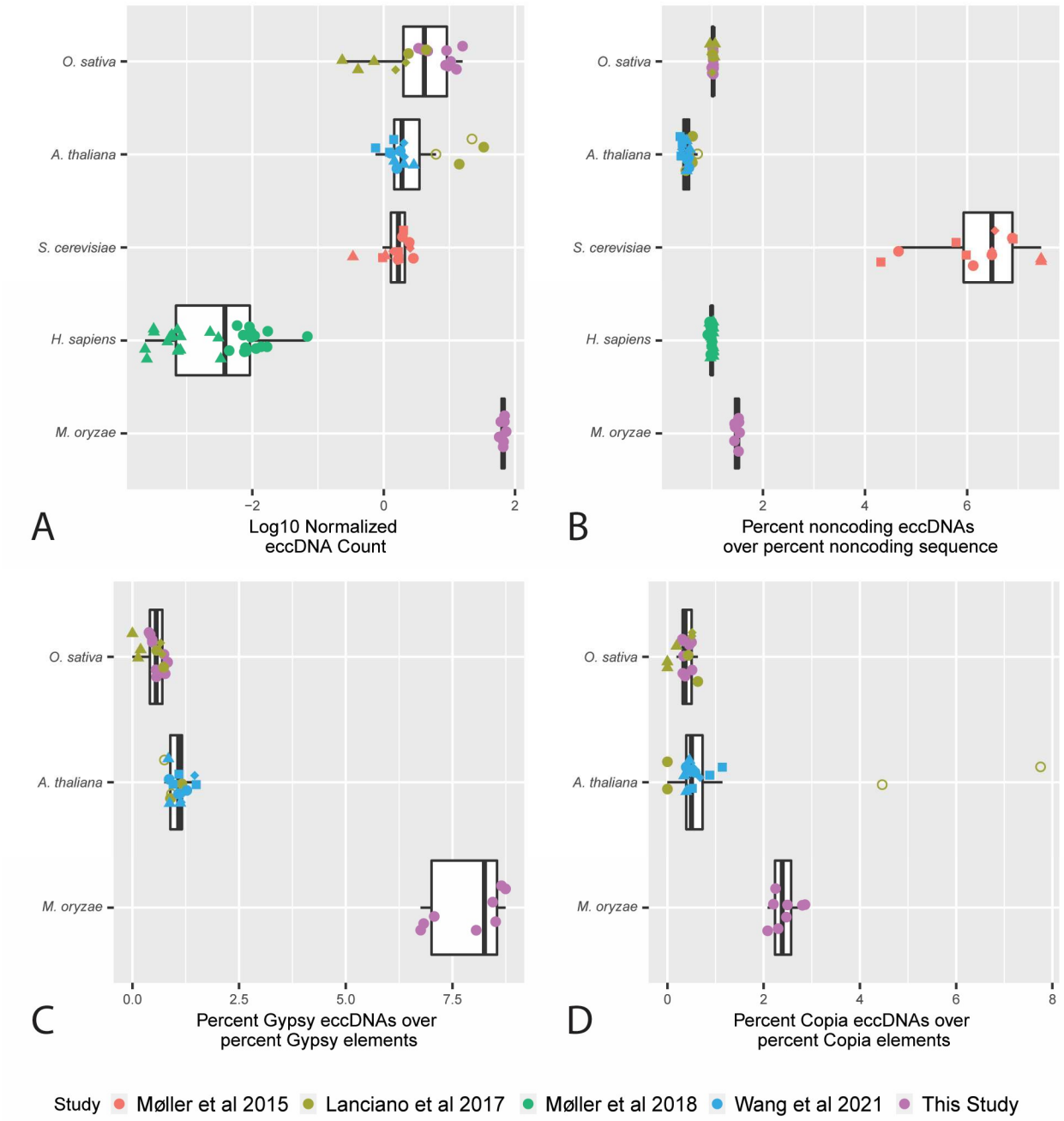

Supplemental Figure 4. Box plots comparing A. log 10 count of eccDNA forming regions normalized to genome size and sequencing library size, B. percent of eccDNA forming regions that contain more than 50% noncoding sequences divided by percent of the genome made up of noncoding seqeuence, C. percent of eccDNA forming regions that contain more than 90% LTR/Gypsy retrotransposon sequence divide by percent of the genome made up of LTR/Gypsy retrotransposon sequence, D. percent of eccDNA forming regions that contain more than 90% LTR/Copia retrotransposon sequence divided by percent of the genome made up of LTR/Gypsy retrotransposon sequence across multiple organisms and studies. Each dot represents one sequenced sample. Shapes represent variations in sample type within the same organism. For *Oryza sativa*, circles represent leaf samples, triangles represent callus samples

882 and diamonds represent seed samples. For *Homo sapiens*, circles represent muscle samples and
883 triangles represent leukocyte samples. For *Arabidopsis thaliana*, circles represent wild type flower
884 samples, empty circles represent *epi12* mutant flower samples, squares represent root samples,
885 diamonds represent leaf samples and triangles represent stem samples. For *Saccharomyces cerevisiae*,
886 circles represent samples from the yeast deletion collection, squares represent samples from the yeast
887 deletion collection treated with zeocin, triangles represent samples from *GAP1* circle carrying yeast,
888 diamonds represent samples from clonal isogenic haploid S228C yeast. For the retrotransposon
889 boxplots, *H. sapiens* samples were excluded due to a lack of active LTR/Gypsy and LTR/Copia
890 retrotransposons in their genome[88] and *S. cerevisiae* samples were excluded due to a small number of
891 eccDNA forming regions containing retrotransposon sequences.

892

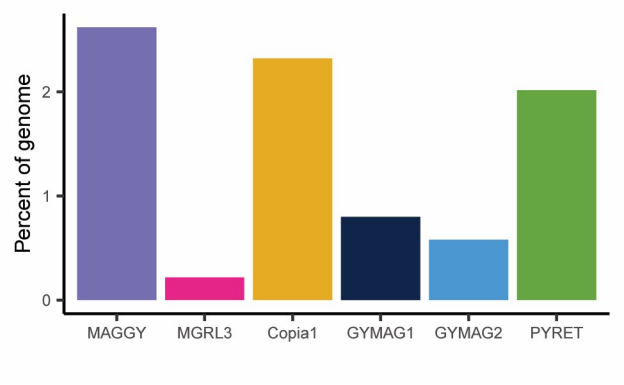

Supplemental Figure 5. Bar plot showing percentage of the *M. oryzae* Guy11 genome made up of each LTR retrotransposon.

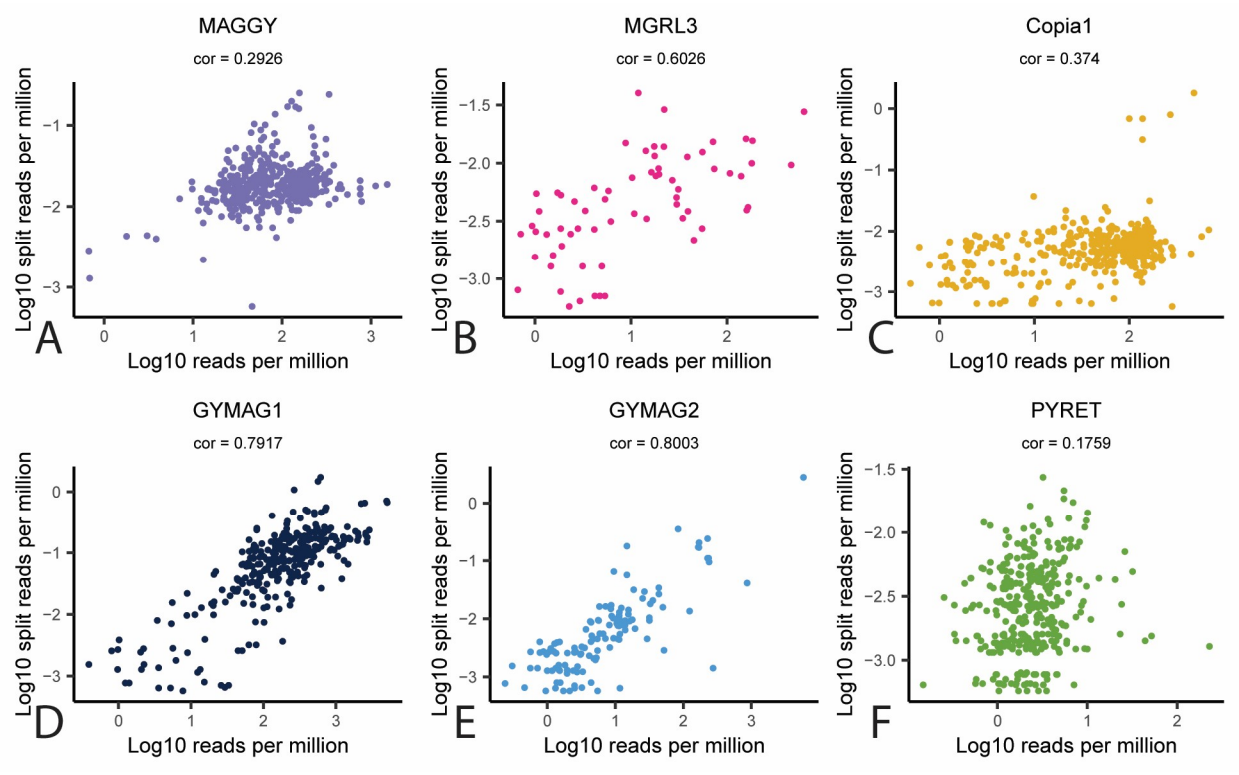

Supplemental Figure 6. A-F. Scatter plots showing Pearson's correlation coefficient between log 10 sequencing reads per million reads and log 10 LTR-LTR split reads per million sequencing reads, averaged across all sequenced samples. Each dot represents one annotated portion of the LTR region of an LTR retrotransposon.

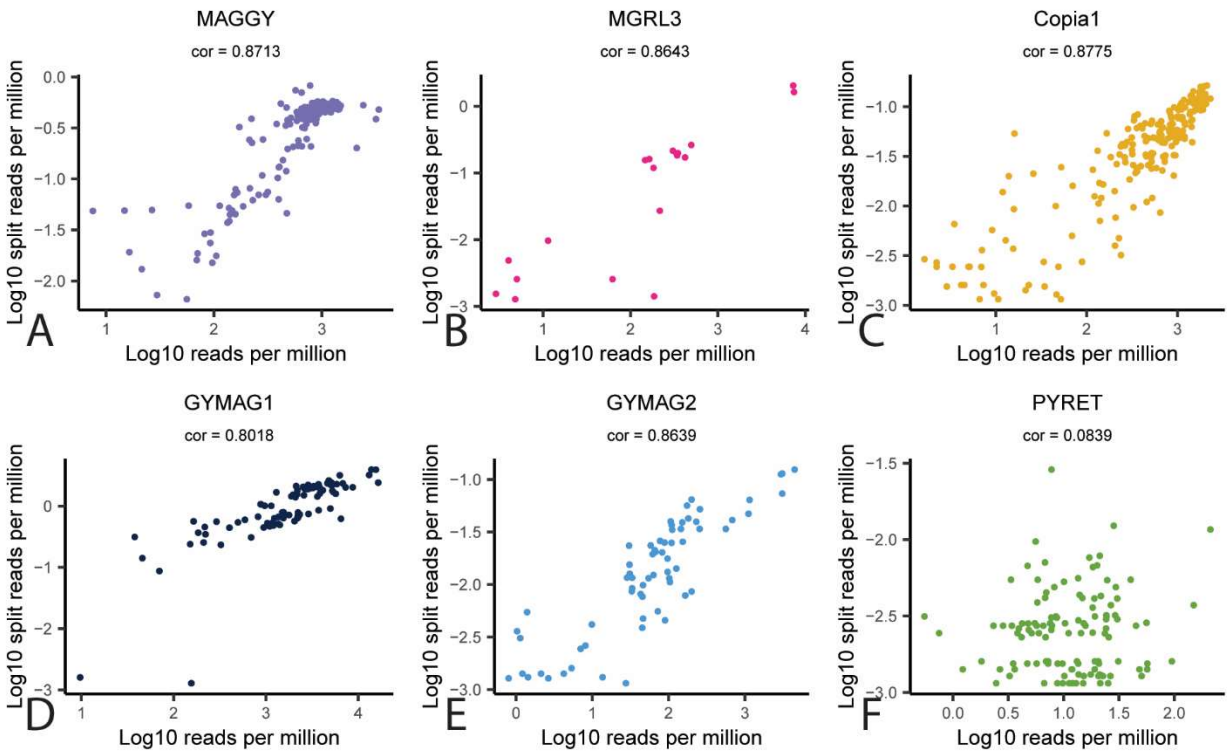

Supplemental figure 7. A-F. Scatter plots showing Pearson's correlation between log 10 sequencing reads per million reads and log 10 LTR-internal split reads per million sequencing reads, averaged across all sequenced samples. Each dot represents one annotated portion of the internal region of an LTR retrotransposon.

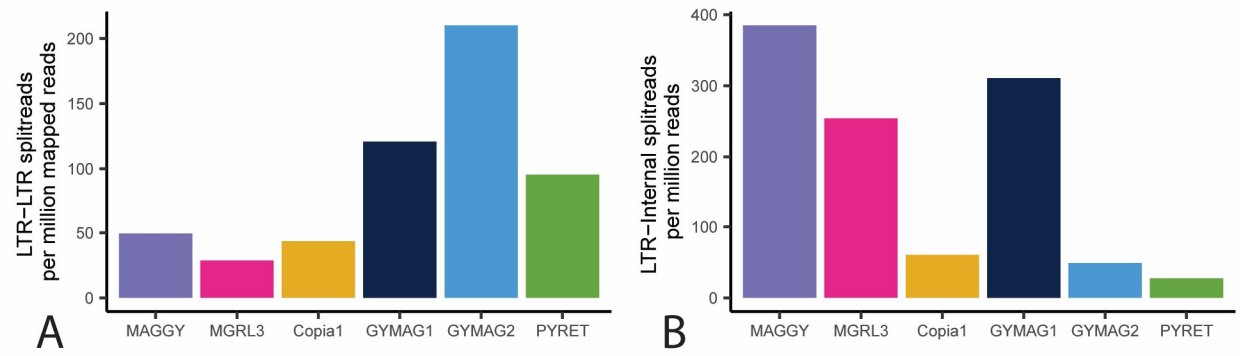

Supplemental Figure 8. A. Bar plot showing identified LTR-LTR split reads per million reads, averaged across all sequenced samples for each LTR retrotransposon in the *M. oryzae* Guy11 genome. B. Bar plot showing identified LTR-internal split reads per million reads, averaged across all sequenced samples for each LTR retrotransposon in the *M. oryzae* Guy11 genome.

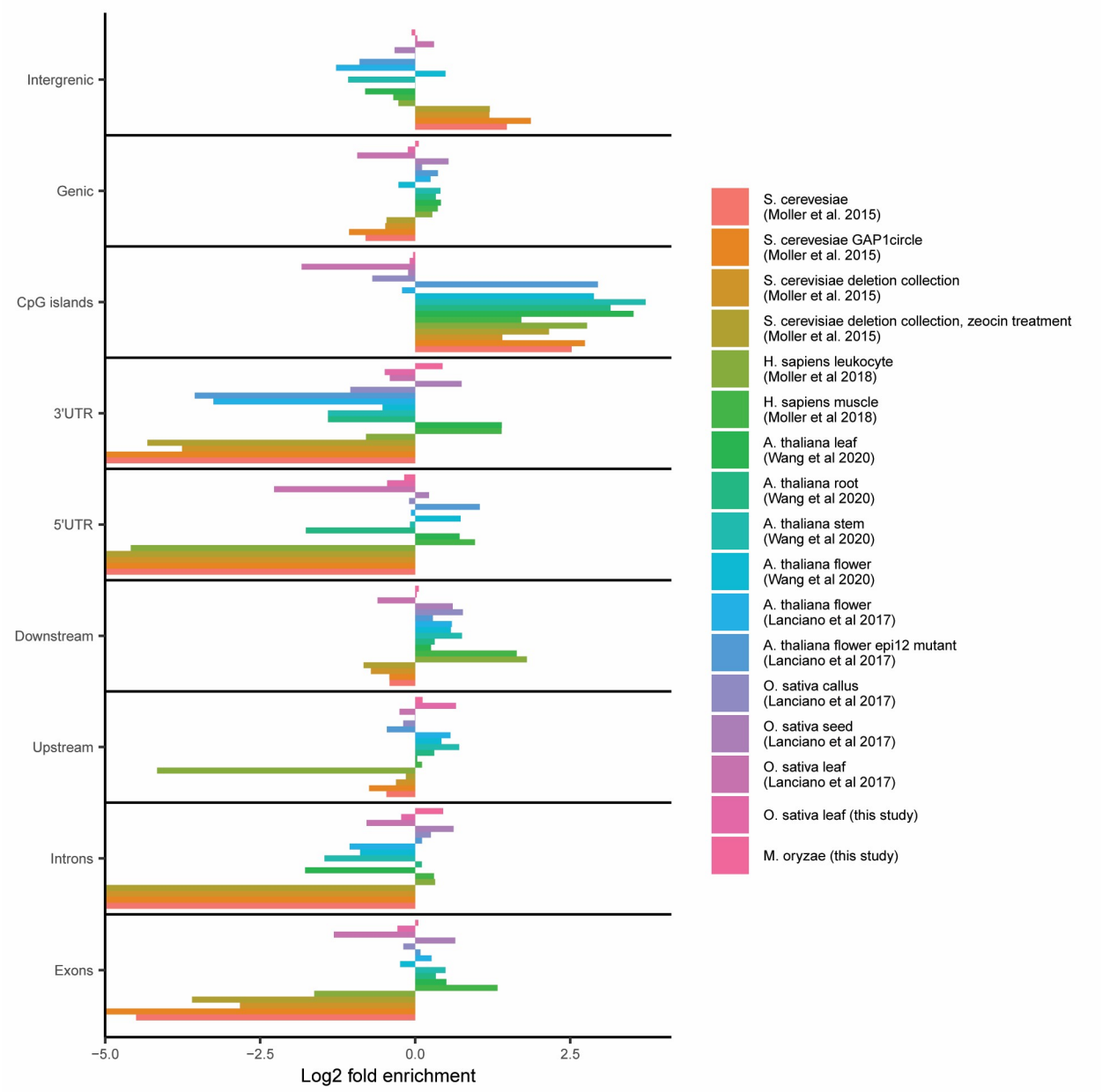

Supplemental Figure 9. Bar plot showing observed enrichment of microDNAs across various regions of the genome across different previously sequenced organisms and sample types. Log2 fold enrichment of -5 represents samples where no microDNAs were found in that region. The presented data is an average of all sequenced samples of each type.

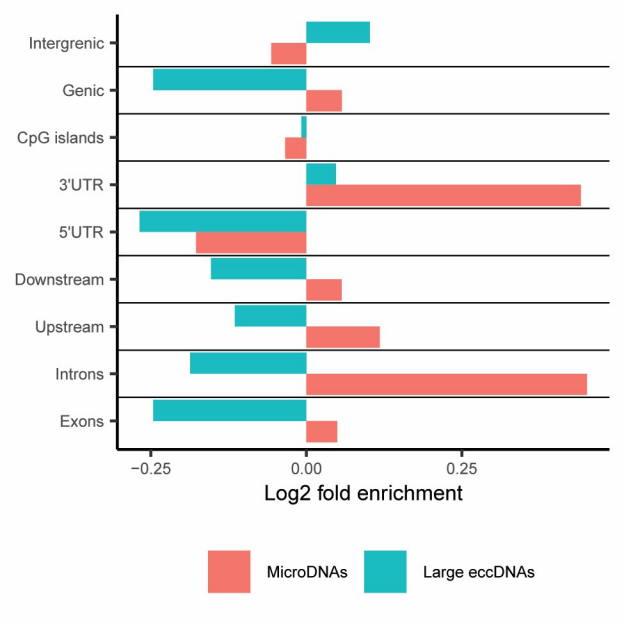

Supplemental Figure 10. Bar plot showing observed enrichment of microDNAs and large eccDNAs across various regions of the genome. The presented data is an average of all sequenced samples from *M. oryzae* Guy11 in this study.

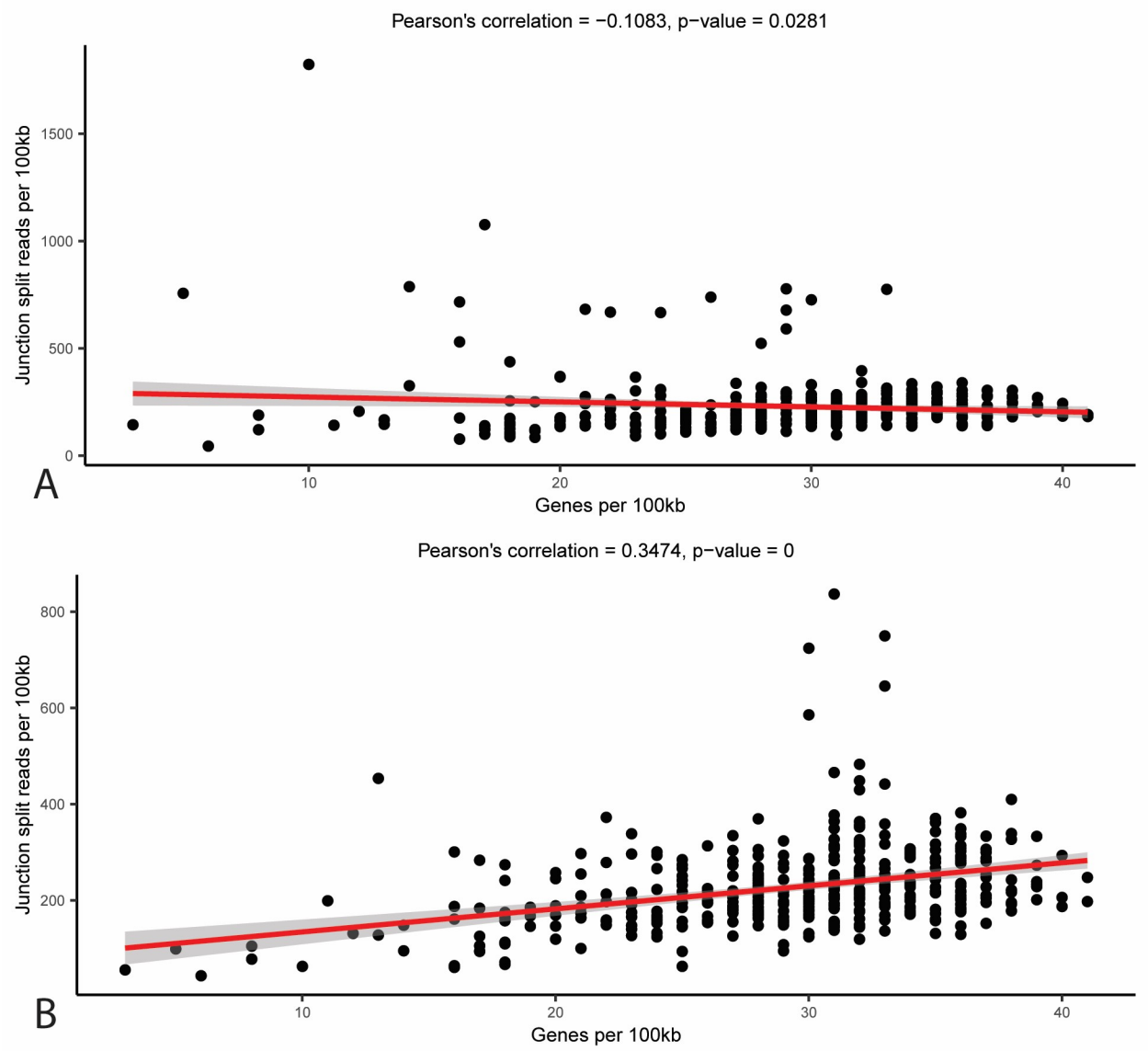

Supplemental Figure 11. Scatter plot showing the number of genes and log 10 of the number of junction split reads per 100 kilobase pair bin in the *M. oryzae* Guy11 genome for A. large eccDNAs or B. microDNAs. The red line represents a linear regression line and the grey shadow represents 95% confidence intervals.

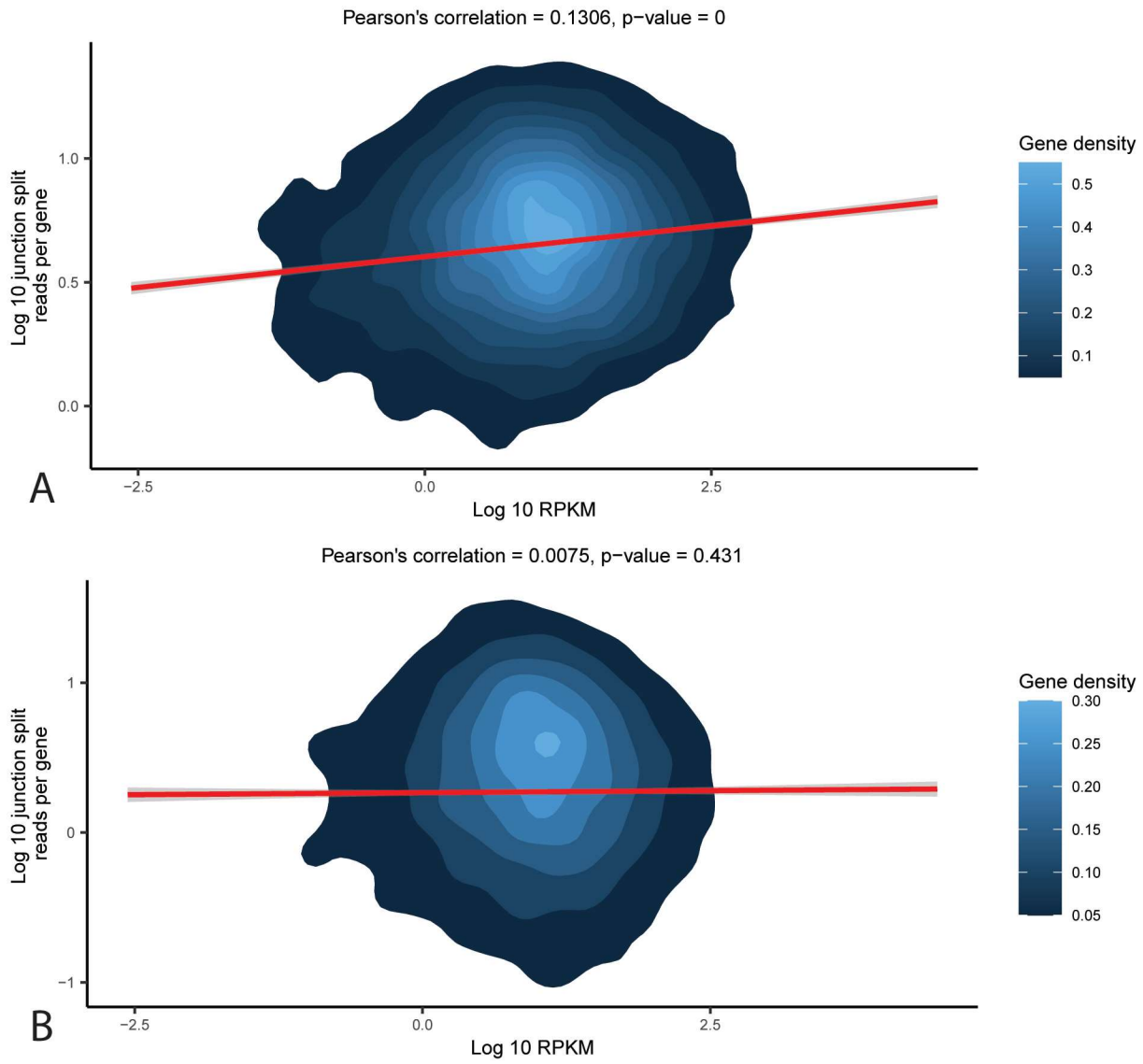

Supplemental Figure 12. Two-dimensional density plot showing the log 10 of the reads per kilobase million averaged across multiple RNAseq samples and log 10 of the number of overlapping junction split reads for each gene for A. large eccDNAs and B. microDNAs. The red line represents a linear regression line and the grey shadow represents 95% confidence intervals.

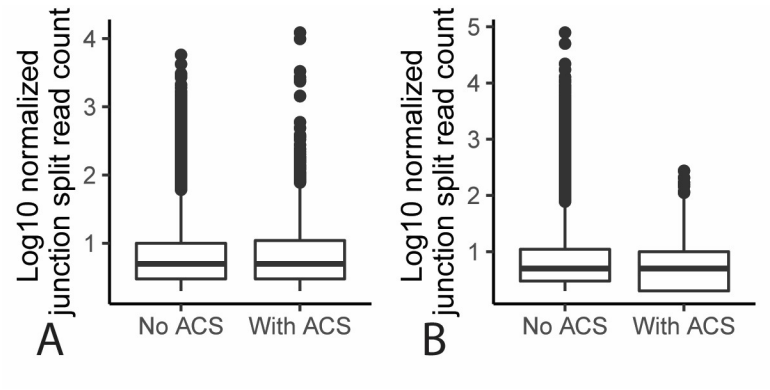

Supplemental Figure 13. Box plot showing the log 10 of the number of junction split reads per million reads averaged across all sequenced samples for eccDNA forming regions that do and do not contain ACSs for A. large eccDNAs and B. microDNAs.

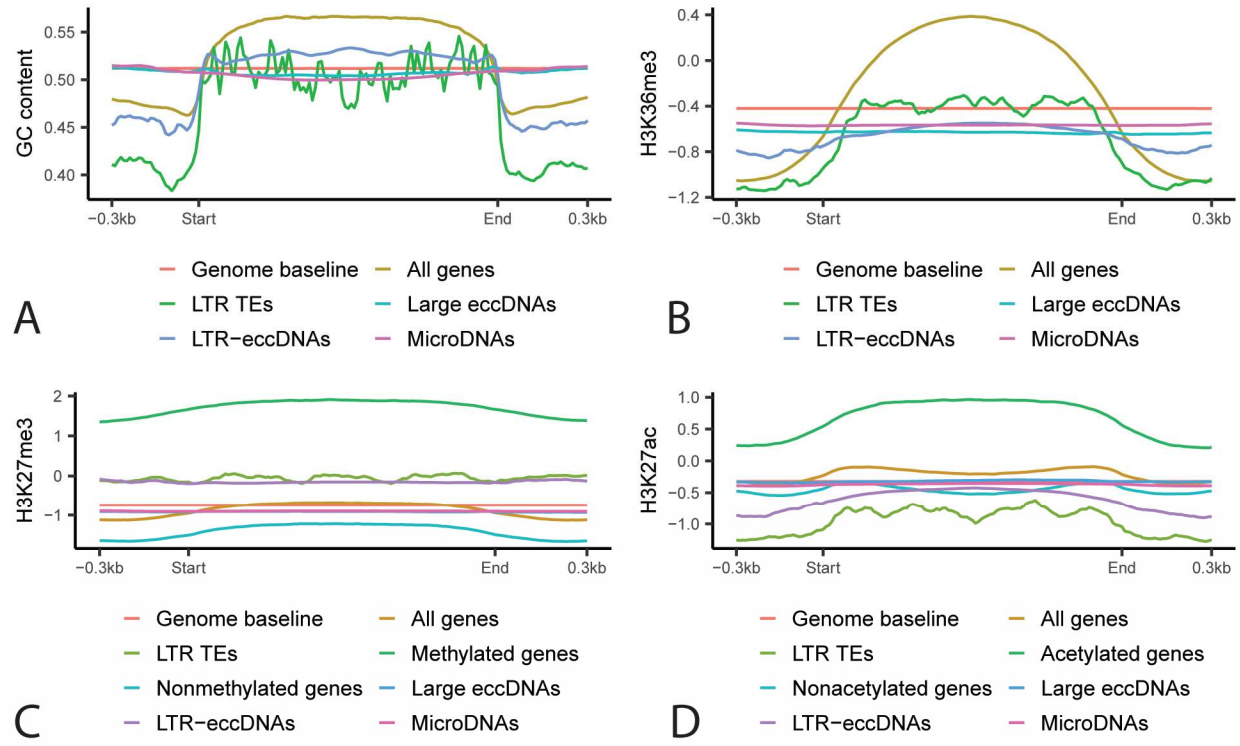

Supplemental Figure 14. Profile plots showing the average A. percent GC content, B. log2 ratio of read coverage for H3K36me3 chromatin immunoprecipitation and input control, C. log2 ratio of read coverage for H3K27me3 chromatin immunoprecipitation and input control and D. log2 ratio between read coverage for H3K27ac chromatin immunoprecipitation and input control for all *M. oryzae* genes, randomly selected regions of the genome, LTR retrotransposons, large eccDNAs, LTR-eccDNAs and microDNAs. Methylated and nonmethylated genes and acetylated and nonacetylated genes are also represented in C and D, respectively.

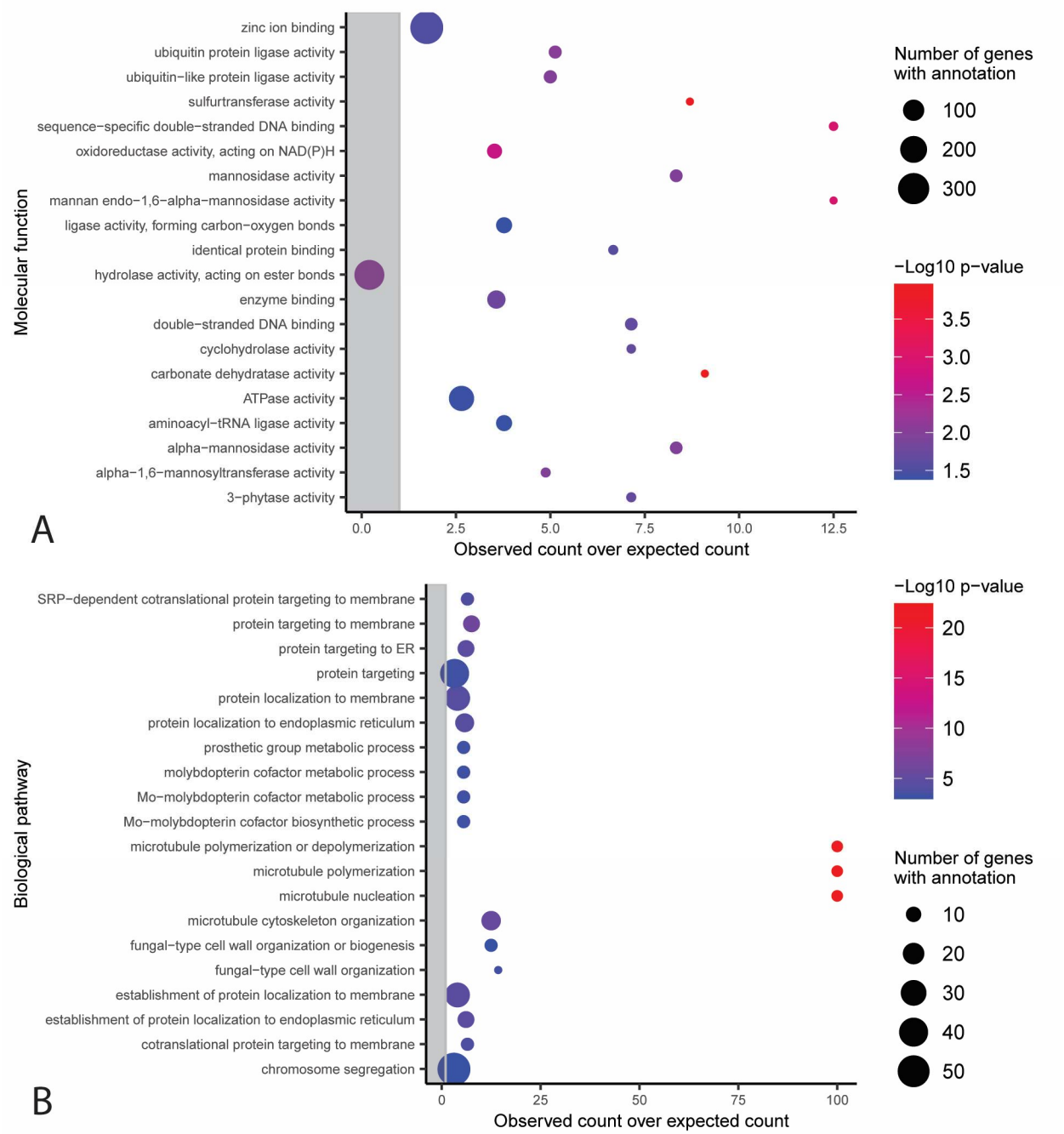

Supplemental Figure 15. Functional categories in the A. molecular function and B. biological pathway Gene Ontology with an observed number of eccDNA-associated genes that is significantly different from the expected number with correction for gene length bias (Chi-square test, $p < 0.05$). The y-axis shows the different functional categories, and the x-axis represents the observed number of genes divided by the expected number of genes in this group. Dots outside of the grey rectangle represent functional categories that are observed more often than expected. The size of dots indicates the total number of genes in the *M. oryzae* genome that belong to each functional category. Only the 20 categories with the largest -log10 p-values are shown.

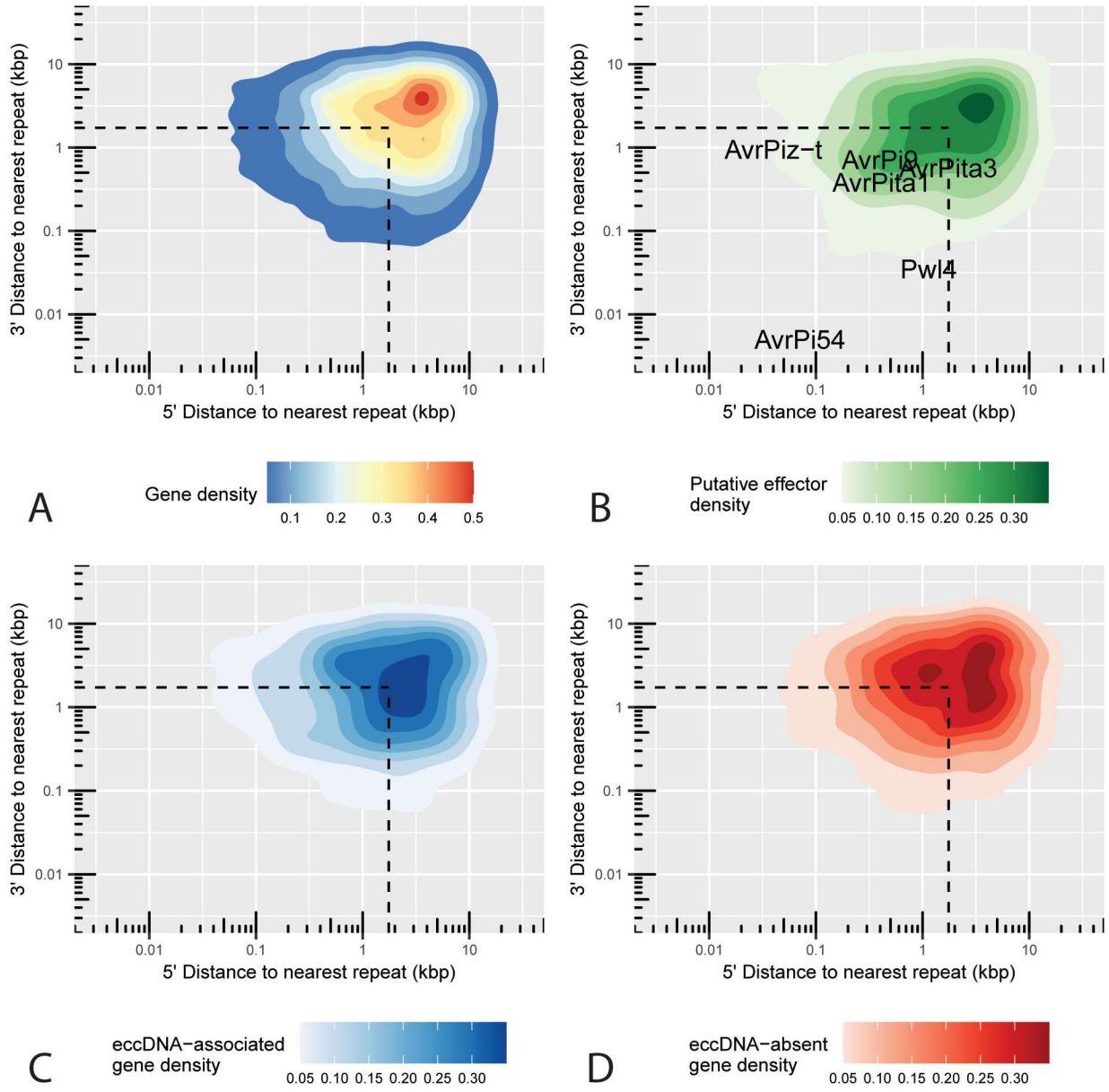

Supplemental Figure 16. Two-dimensional density plot representing the 5’ and 3’ distance to the nearest repeat in the *M. oryzae* Guy11 genome in kilobase pairs for each A. gene, B. predicted effector, C. eccDNA-associated genes, and D. eccDNA-absent genes. Known effectors are shown as text in B. Dashed lines represent median 5’ and 3’ distance to nearest gene.

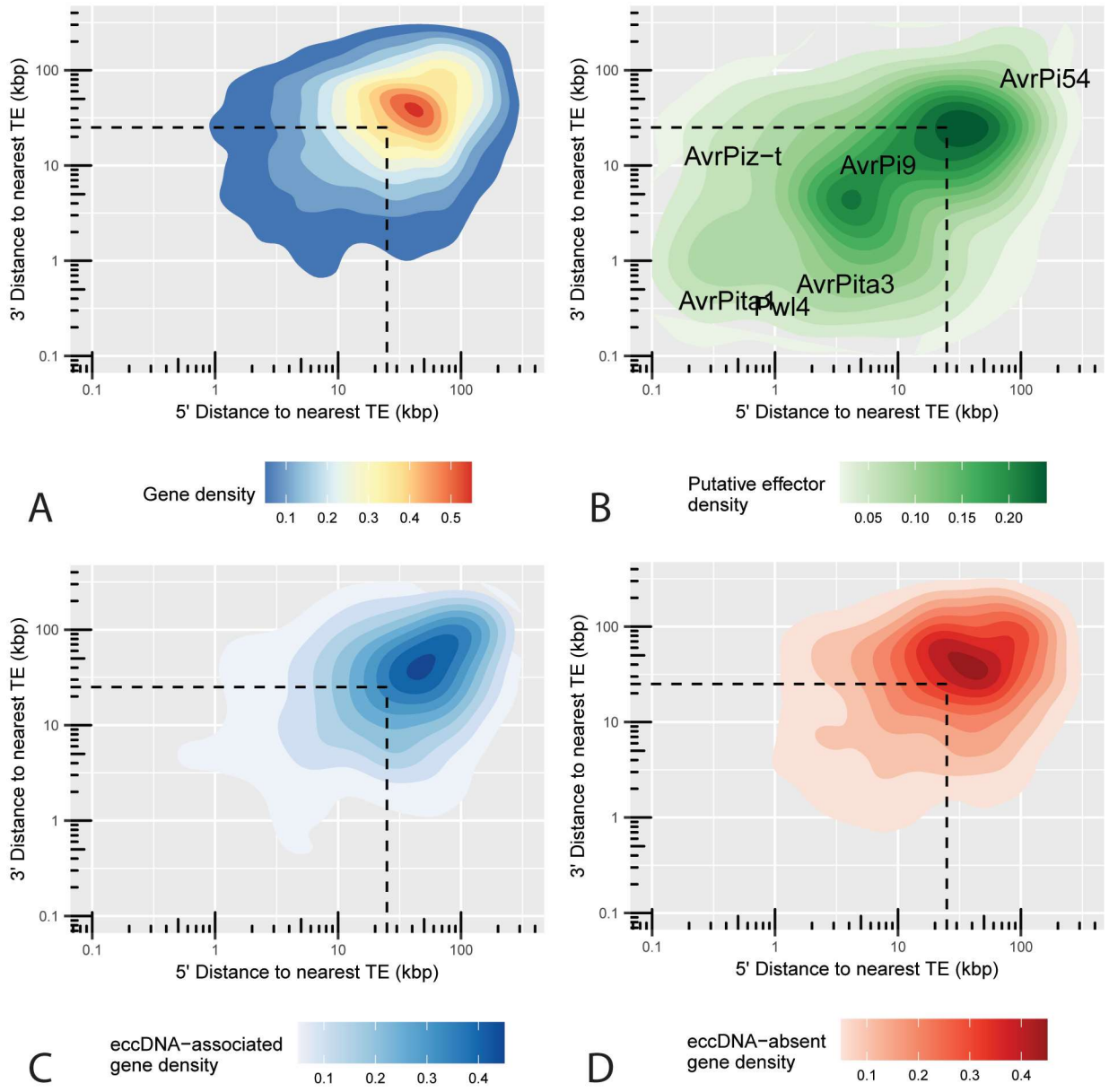

Supplemental Figure 17. Two-dimensional density plot representing the 5' and 3' distance to the nearest transposable element in the *M. oryzae* Guy11 genome in kilobase pairs for each A. gene, B. predicted effector, C. eccDNA-associated genes, and D. eccDNA-absent genes. Known effectors are shown as text in B. Dashed lines represent median 5' and 3' distance to nearest gene.

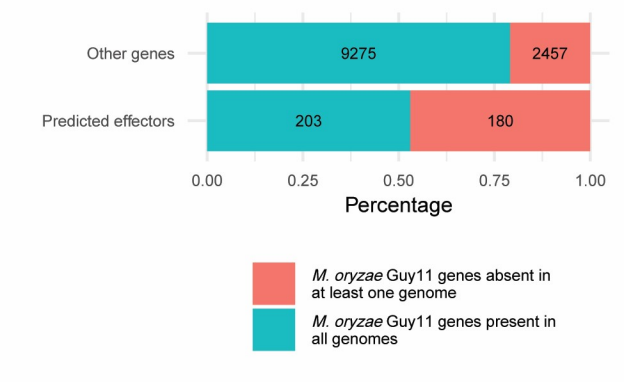

Supplemental Figure 18. Stacked bar plot showing the percentage of predicted effectors and all other genes in the *M. oryzae* Guy11 genome that had an ortholog in all other 162 *M. oryzae* genomes analyzed or not. Numbers indicate the number of genes in each category.

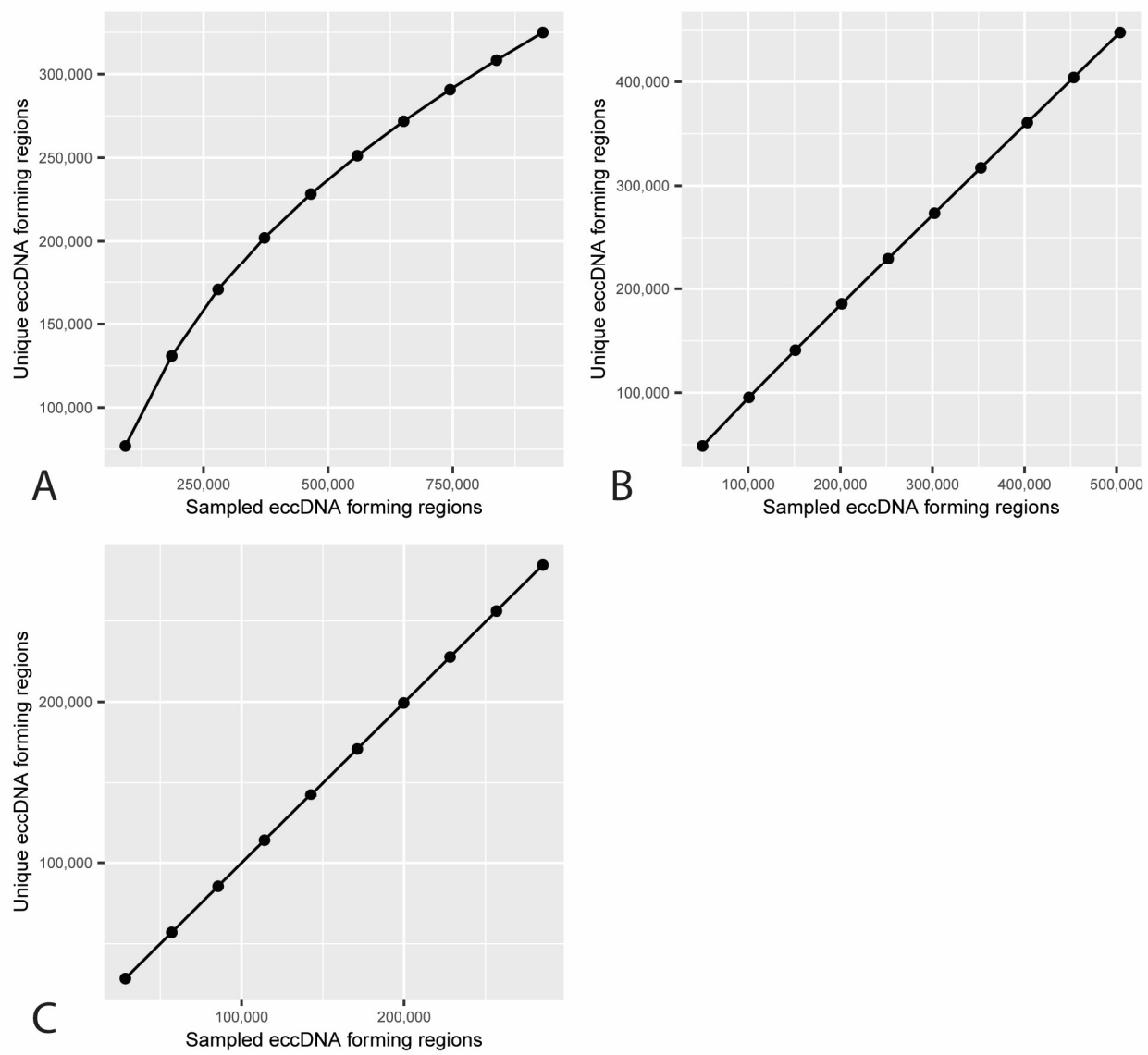

971 **Supplemental Figure 19.** Rarefaction analysis of the number of unique eccDNA forming regions at
972 different subsamples of eccDNA forming regions across all samples for A. LTR-eccDNAs, B. large eccDNAs
973 and C. microDNAs.

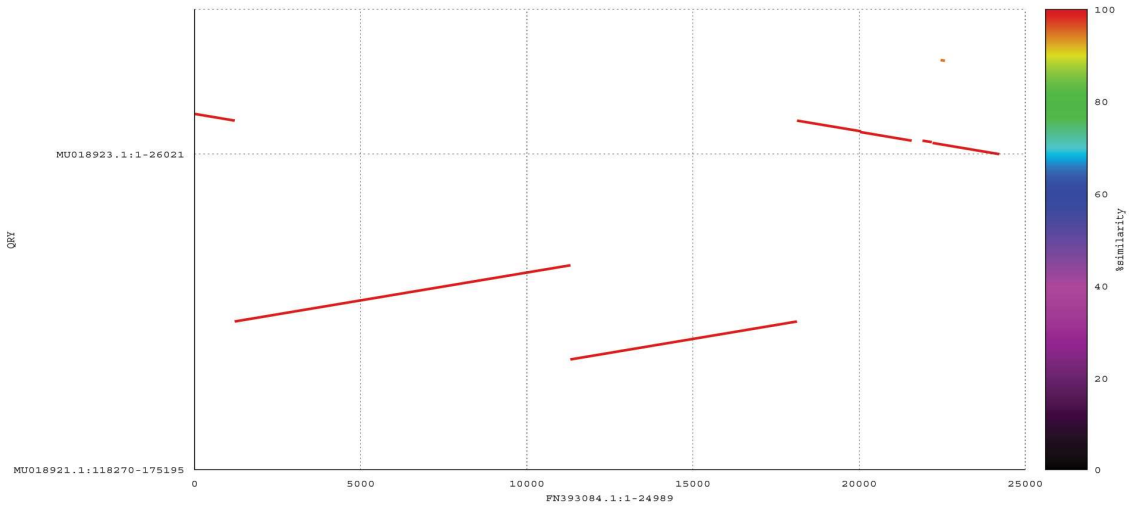

A

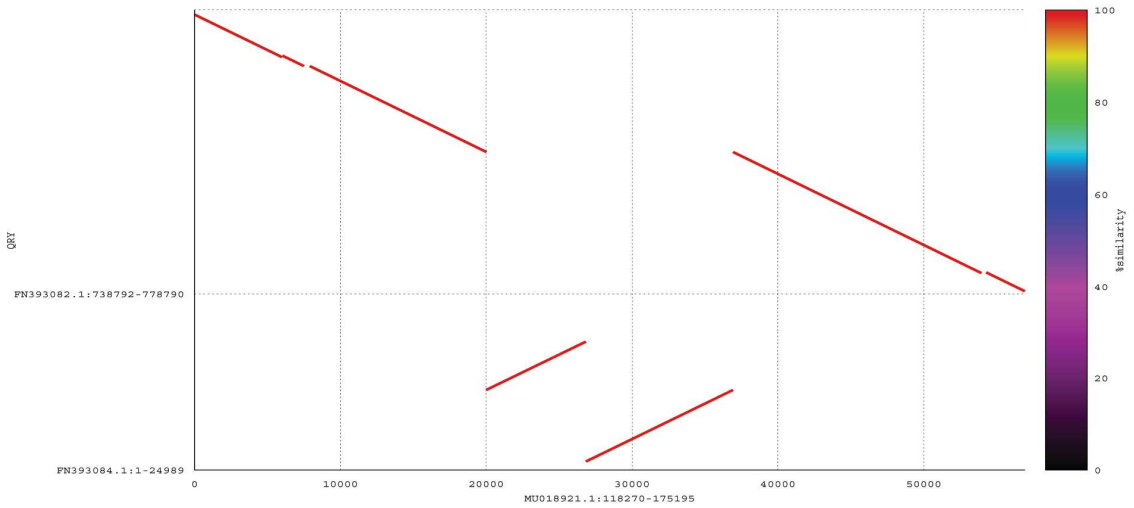

B

974

975 **Supplemental Figure 20.** Dot plot alignments between *S. cerevisiae* M22 and *S. cerevisiae* EC1118
976 genomes showing a DNA translocation likely caused by an eccDNA intermediate in yeast. A. A scaffold of
977 the EC1118 genome aligns to two different scaffolds of the M22 genome. B. A scaffold of the M22
978 genome aligns to two different scaffolds of the EC1118 genome.

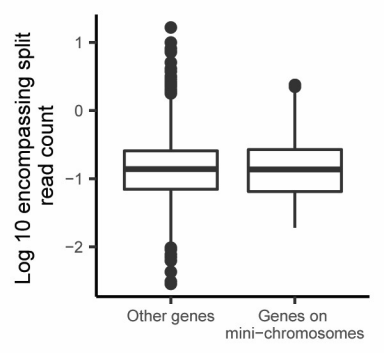

979

980 **Supplemental Figure 21.** Box plot showing the log 10 of the number of junction split reads per million
981 reads averaged across all sequenced samples that fully encompass genes previously found on mini-
982 chromosomes in other strains of *M. oryzae* and other genes.

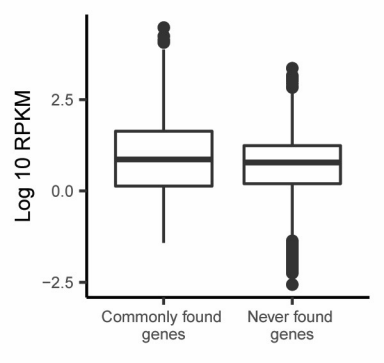

983

984 **Supplemental Figure 22.** Box plot showing the log 10 reads per kilobase million (RPKM) averaged over
985 12 previously published RNAseq samples for eccDNA-associated genes and eccDNA-absent genes.

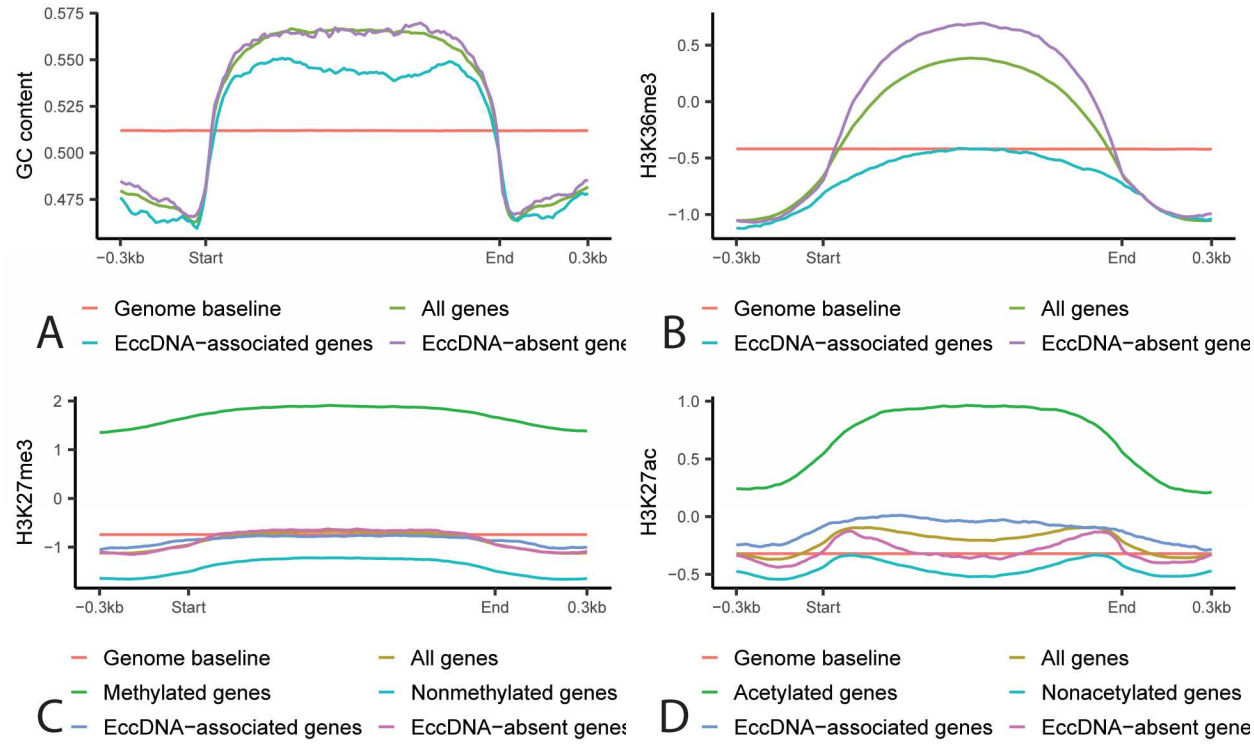

Supplemental Figure 23. Profile plots showing the average A. percent GC content, B., log2 ratio between read coverage for H3K36me3 chromatin immunoprecipitation and input control, C. log2 ratio between read coverage for H3K27me3 chromatin immunoprecipitation and input control and D. log2 ratio between read coverage for H3K27ac chromatin immunoprecipitation and input control for all *M. oryzae* genes, randomly selected regions of the genome, eccDNA-associated genes, and eccDNA-absent genes. Methylated and nonmethylated genes and acetylated and nonacetylated genes are also represented in C and D, respectively.

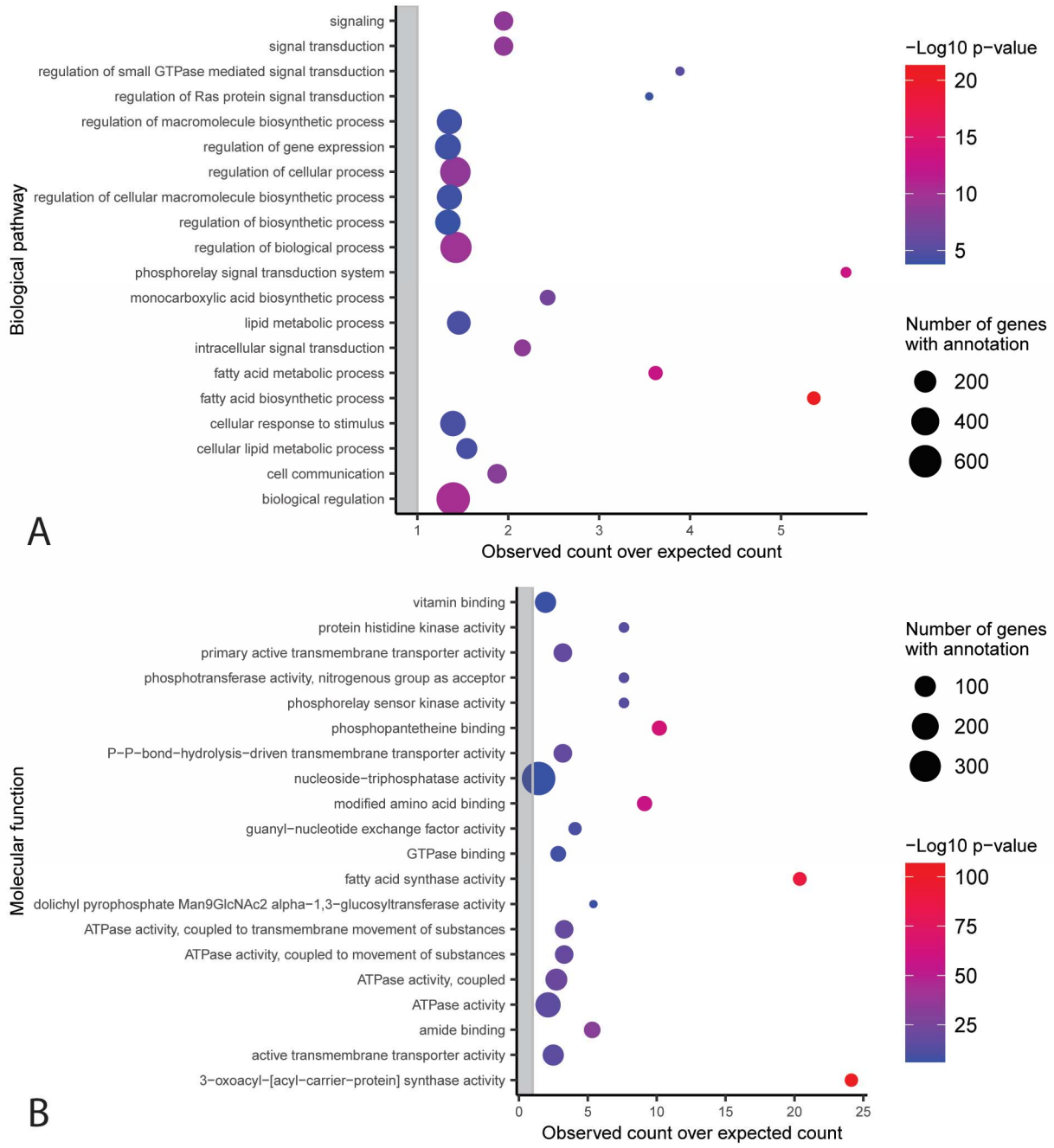

Supplemental Figure 24. Functional categories in the A. molecular function and B. biological pathway Gene Ontology with an observed number of eccDNA-absent genes that is significantly different from the expected number with correction for gene length bias (Chi-square test, $p < 0.05$). The y-axis shows the different functional categories, and the x-axis represents the observed number of genes divided by the expected number of genes in this group. Dots outside of the grey rectangle represent functional categories that are observed more often than expected. The size of dots indicates the total number of genes in the *M. oryzae* genome that belong to each functional category. Only the 20 categories with the largest -log10 p-values are shown.

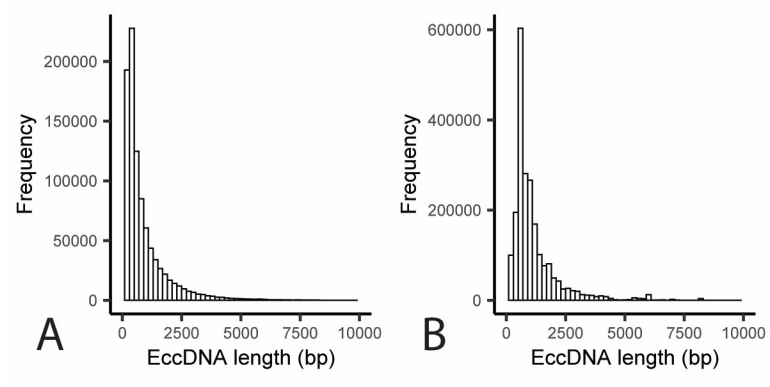

Supplemental Figure 25. Histogram showing the distribution of candidate eccDNA forming regions in *M. oryzae* for one sequenced sample. A. Length distribution of candidate eccDNA forming regions inferred from uniquely mapped reads. B. Length distribution of candidate eccDNA forming regions inferred from multi-mapping reads.

1008 **Supplemental Tables**

Accessions	Read count	EccDNA forming regions	Junction split reads	False positives per million reads
ERR2660591	222500000.	12.00	195.0	0.8765
ERR5060418	73760000.	15.00	210.0	2.847
SRR11528297	168600000.	5.000	66.00	0.3915

1009

1010 **Supplemental Table 1.** Read count, eccDNA forming regions inferred and number of junction split reads
1011 found using our pipeline on three previously published whole genome sequencing datasets for *M.*
1012 *oryzae*.

1013

Study	DNA extraction	Column purification	Linear DNA degradation	Circular DNA amplification
Moller et al 2015	Plasmid Mini AX (A&A Biotechnology)	Plasmid Mini AX (A&A Biotechnology)	Plasmid-Safe ATP-dependent DNase (Epicentre); NotI (Fermentas)	REPLI-g Mini Kit (Qiagen)
Lanciano et al 2017	Plant DNeasy mini kit (Qiagen)	Geneclean kit (MPBio)	Plasmid-Safe ATP-dependent DNase, (Epicentre)	Illustra TempliPhi kit (GE Healthcare)
Moller et al 2018	Plasmid Mini AX (A&A Biotechnology)	Plasmid Mini AX (A&A Biotechnology)	Plasmid-Safe ATP-dependent DNase (Epicentre); MssI (Thermo Scientific)	REPLI-g Midi Kit (Qiagen)
Wang et al 2021	Plant DNeasy mini kit (Qiagen)	Geneclean kit (MPBio)	Plasmid-Safe ATP-dependent DNase (Epicentre)	REPLI-g Mini Kit (Qiagen)
This Study (Magnaporthe oryzae)	SDS and KAc extraction	DNA Clean and Concentrator-5 Kit (Zymo Research)	Plasmid-Safe ATP-dependent DNase (Epicentre)	Illustra TempliPhi kit (GE Healthcare)
This Study (Oryza sativa)	Plant DNeasy mini kit (Qiagen)	DNA Clean and Concentrator-5 Kit (Zymo Research)	Plasmid-Safe ATP-dependent DNase (Epicentre)	Illustra TempliPhi kit (GE Healthcare)

1014

1015 **Supplemental Table 2.** DNA extraction kit, column purification kit, linear DNA degradation enzymes and
1016 circular DNA amplification enzymes used for all studies whose data was used to compare the
1017 circularomes of the organisms discussed in this study.

1018

1019 **Supplemental Data Files**

1020 **Supplemental Data File 1.** List of eccDNA forming regions called using Illumina circularome sequencing
1021 data for *M. oryzae* in this study. The first column describes the sample the eccDNA forming region was
1022 called with, the next three columns represent the genomic coordinates of the eccDNA forming region,
1023 and the last column represents the number of junction split reads used to call the eccDNA forming
1024 region.

1025 **Supplemental Data File 2.** List of eccDNA forming regions called using PacBio circularome sequencing
1026 data for *M. oryzae* in this study. The first column describes the sample the eccDNA forming region was
1027 called with, the next three columns represent the genomic coordinates of the eccDNA forming region,
1028 and the last column represents the number of junction split reads used to call the eccDNA forming
1029 region.

1030 **Supplemental Data File 3.** List of eccDNA forming regions called using Illumina circularome sequencing
1031 data for *O. sativa* in this study. The first column describes the sample the eccDNA forming region was
1032 called with, the next three columns represent the genomic coordinates of the eccDNA forming region,
1033 and the last column represents the number of junction split reads used to call the eccDNA forming
1034 region.

1035 **Supplemental Data File 4.** List of eccDNA forming regions called using Illumina circularome sequencing
1036 data for *O. sativa* leaf tissue published by Lanciano et al[27]. The first column describes the sample the
1037 eccDNA was called with, the next three columns represent the genomic coordinates of the eccDNA
1038 forming region, and the last column represents the number of junction split reads used to call the
1039 eccDNA forming region.

1040 **Supplemental Data File 5.** List of eccDNA forming regions called using Illumina circularome sequencing
1041 data for *O. sativa* seed tissue published by Lanciano et al[27]. The first column describes the sample the
1042 eccDNA was called with, the next three columns represent the genomic coordinates of the eccDNA
1043 forming region, and the last column represents the number of junction split reads used to call the
1044 eccDNA forming region.

1045 **Supplemental Data File 6.** List of eccDNA forming regions called using Illumina circularome sequencing
1046 data for *O. sativa* callus tissue published by Lanciano et al[27]. The first column describes the sample the
1047 eccDNA was called with, the next three columns represent the genomic coordinates of the eccDNA
1048 forming region, and the last column represents the number of junction split reads used to call the
1049 eccDNA forming region.

1050 **Supplemental Data File 7.** List of eccDNA forming regions called using Illumina circularome sequencing
1051 data for *A. thaliana* WT tissue published by Lanciano et al[27]. The first column describes the sample the
1052 eccDNA was called with, the next three columns represent the genomic coordinates of the eccDNA
1053 forming region, and the last column represents the number of junction split reads used to call the
1054 eccDNA forming region.

1055 **Supplemental Data File 8.** List of eccDNA forming regions called using Illumina circularome sequencing
1056 data for *A. thaliana epi12* mutant tissue published by Lanciano et al[27]. The first column describes the
1057 sample the eccDNA was called with, the next three columns represent the genomic coordinates of the

1058 eccDNA forming region, and the last column represents the number of junction split reads used to call
1059 the eccDNA forming region.

1060 **Supplemental Data File 9.** List of eccDNA forming regions called using Illumina circularome sequencing
1061 data for *A. thaliana* leaf tissue published by Wang et al[32]. The first column describes the sample the
1062 eccDNA was called with, the next three columns represent the genomic coordinates of the eccDNA
1063 forming region, and the last column represents the number of junction split reads used to call the
1064 eccDNA forming region.

1065 **Supplemental Data File 10.** List of eccDNA forming regions called using Illumina circularome sequencing
1066 data for *A. thaliana* root tissue published by Wang et al[32]. The first column describes the sample the
1067 eccDNA was called with, the next three columns represent the genomic coordinates of the eccDNA
1068 forming region, and the last column represents the number of junction split reads used to call the
1069 eccDNA forming region.

1070 **Supplemental Data File 11.** List of eccDNA forming regions called using Illumina circularome sequencing
1071 data for *A. thaliana* stem tissue published by Wang et al[32]. The first column describes the sample the
1072 eccDNA was called with, the next three columns represent the genomic coordinates of the eccDNA
1073 forming region, and the last column represents the number of junction split reads used to call the
1074 eccDNA forming region.

1075 **Supplemental Data File 12.** List of eccDNA forming regions called using Illumina circularome sequencing
1076 data for *A. thaliana* flower tissue published by Wang et al[32]. The first column describes the sample the
1077 eccDNA was called with, the next three columns represent the genomic coordinates of the eccDNA
1078 forming region, and the last column represents the number of junction split reads used to call the
1079 eccDNA forming region.

1080 **Supplemental Data File 13.** List of eccDNA forming regions called using Illumina circularome sequencing
1081 data for *H. sapiens* muscle tissue published by Møller et al[11]. The first column describes the sample the
1082 eccDNA was called with, the next three columns represent the genomic coordinates of the eccDNA
1083 forming region, and the last column represents the number of junction split reads used to call the
1084 eccDNA forming region.

1085 **Supplemental Data File 14.** List of eccDNA forming regions called using Illumina circularome sequencing
1086 data for *H. sapiens* leukocytes published by Møller et al[11]. The first column describes the sample the
1087 eccDNA was called with, the next three columns represent the genomic coordinates of the eccDNA
1088 forming region, and the last column represents the number of junction split reads used to call the
1089 eccDNA forming region.

1090 **Supplemental Data File 15.** List of eccDNA forming regions called using Illumina circularome sequencing
1091 data for *S. cerevisiae* WT cells published by Møller et al[11]. The first column describes the sample the
1092 eccDNA was called with, the next three columns represent the genomic coordinates of the eccDNA
1093 forming region, and the last column represents the number of junction split reads used to call the
1094 eccDNA forming region.

1095 **Supplemental Data File 16.** List of eccDNA forming regions called using Illumina circularome sequencing
1096 data for *S. cerevisiae* GAP1^{circle} cells published by Møller et al[28]. The first column describes the sample
1097 the eccDNA was called with, the next three columns represent the genomic coordinates of the eccDNA

1098 forming region, and the last column represents the number of junction split reads used to call the
1099 eccDNA forming region.

1100 **Supplemental Data File 17.** List of eccDNA forming regions called using Illumina circularome sequencing
1101 data for *S. cerevisiae* cells from the deletion collection published by Møller et al[28]. The first column
1102 describes the sample the eccDNA was called with, the next three columns represent the genomic
1103 coordinates of the eccDNA forming region, and the last column represents the number of junction split
1104 reads used to call the eccDNA forming region.

1105 **Supplemental Data File 18.** List of eccDNA forming regions called using Illumina circularome sequencing
1106 data for *S. cerevisiae* cells from the deletion collection treated with zeocin published by Møller et al[28].
1107 The first column describes the sample the eccDNA was called with, the next three columns represent the
1108 genomic coordinates of the eccDNA forming region, and the last column represents the number of
1109 junction split reads used to call the eccDNA forming region.

1110 **Supplemental Data File 19.** List of genes annotated in the *M. oryzae* Guy11 genome along with other
1111 information discussed in this study for each gene. The first three columns describe the genomic
1112 coordinates of the gene, the fourth column is the gene's ID, the fifth column describes whether the gene
1113 was predicted to be an effector, the sixth column lists its name if it is a known effector, the seventh
1114 column lists the name of the protein in the *M. oryzae* 70-15 proteome, the eighth column describes
1115 whether it is an eccDNA-associated or eccDNA-absent gene, and the last column describes whether this
1116 gene was kept in all rice-infecting *M. oryzae* genomes analyzed.

1117 **Supplemental Data File 20.** Enriched GO terms in the cellular components ontology for eccDNA-
1118 associated genes. The first column lists the GO term, the second column lists the number of genes
1119 annotated with each term, the third column lists the number of genes observed in the eccDNA-
1120 associated category, the fourth column list the number of genes expected in that category, the fifth
1121 column shows is a description of the go term, the sixth column lists the Chi-square value for that GO
1122 term, and the final column lists the ratio of the observed number of genes in the eccDNA-associated
1123 category divided by the expected number of genes in that category.

1124 **Supplemental Data File 21.** Enriched GO terms in the molecular function ontology for eccDNA-
1125 associated genes. The first column lists the GO term, the second column lists the number of genes
1126 annotated with each term, the third column lists the number of genes observed in the eccDNA-
1127 associated category, the fourth column list the number of genes expected in that category, the fifth
1128 column shows is a description of the go term, the sixth column lists the Chi-square value for that GO
1129 term, and the final column lists the ratio of the observed number of genes in the eccDNA-associated
1130 category divided by the expected number of genes in that category.

1131 **Supplemental Data File 22.** Enriched GO terms in the biological pathway ontology for eccDNA-
1132 associated genes. The first column lists the GO term, the second column lists the number of genes
1133 annotated with each term, the third column lists the number of genes observed in the eccDNA-
1134 associated category, the fourth column list the number of genes expected in that category, the fifth
1135 column shows is a description of the go term, the sixth column lists the Chi-square value for that GO
1136 term, and the final column lists the ratio of the observed number of genes in the eccDNA-associated
1137 category divided by the expected number of genes in that category.

1138 **Supplemental Data File 23.** List of GenBank accessions for the genomes of rice-infecting *M. oryzae*
1139 isolates used in this study for gene annotation.

1140 **Supplemental Data File 24.** Small, genic deletions identified in the *M. oryzae* Guy11 genome. The first
1141 three columns describe genomic coordinates of the deletion, the fourth column is the missing gene's ID,
1142 and the last column is the name of the genome where the deletion is present.

1143 **Supplemental Data File 25.** List of GenBank accessions for the genomes of *M. oryzae* used in this study
1144 to search for eccDNA-mediated translocations.

1145 **Supplemental Data File 26.** Enriched GO terms in the cellular components ontology for eccDNA-absent
1146 genes. The first column lists the GO term, the second column lists the number of genes annotated with
1147 each term, the third column lists the number of genes observed in the eccDNA-absent category, the
1148 fourth column list the number of genes expected in that category, the fifth column shows is a
1149 description of the go term, the sixth column lists the Chi-square value for that GO term, and the final
1150 column lists the ratio of the observed number of genes in the eccDNA-associated category divided by
1151 the expected number of genes in that category.

1152 **Supplemental Data File 27.** Enriched GO terms in the molecular function ontology for eccDNA-absent
1153 genes. The first column lists the GO term, the second column lists the number of genes annotated with
1154 each term, the third column lists the number of genes observed in the eccDNA-absent category, the
1155 fourth column list the number of genes expected in that category, the fifth column shows is a
1156 description of the go term, the sixth column lists the Chi-square value for that GO term, and the final
1157 column lists the ratio of the observed number of genes in the eccDNA-associated category divided by
1158 the expected number of genes in that category.

1159 **Supplemental Data File 28.** Enriched GO terms in the biological pathway ontology for eccDNA-absent
1160 genes. The first column lists the GO term, the second column lists the number of genes annotated with
1161 each term, the third column lists the number of genes observed in the eccDNA-absent category, the
1162 fourth column list the number of genes expected in that category, the fifth column shows is a
1163 description of the go term, the sixth column lists the Chi-square value for that GO term, and the final
1164 column lists the ratio of the observed number of genes in the eccDNA-associated category divided by
1165 the expected number of genes in that category.

1166 **Supplemental Data File 29.** Consensus sequences of LTR retrotransposons in the *M. oryzae* Guy11
1167 genome in FASTA format.

1168 **Supplemental Data File 30.** Genome, gene annotation, and transposable element annotation files used
1169 for comparative circularome analysis.

1170 **Supplemental Data File 31.** List of SRA accessions for RNAseq data used in this study.

1171

1172 **References**

1173 1. Paulsen, T., Kumar, P., Koseoglu, M. M. & Dutta, A. Discoveries of Extrachromosomal Circles of
1174 DNA in Normal and Tumor Cells. *Trends Genet.* **34**, 270–278 (2018).

1175 2. Kilzer, J. M. *et al.* Roles of host cell factors in circularization of retroviral DNA. *Virology* **314**, 460–
1176 467 (2003).

1177 3. Garfinkel, D. J. *et al.* Retrotransposon Suicide: Formation of Ty1 Circles and Autointegration via a
1178 Central DNA Flap. *J. Virol.* **80**, 11920–11934 (2006).

1179 4. Møller, H. D. *et al.* Formation of extrachromosomal circular DNA from long terminal repeats of
1180 retrotransposons in Saccharomyces cerevisiae. *G3 Genes, Genomes, Genet.* **6**, 453–462 (2016).

1181 5. Gresham, D. *et al.* Adaptation to diverse nitrogen-limited environments by deletion or
1182 extrachromosomal element formation of the GAP1 locus. *Proc. Natl. Acad. Sci.* **107**, 18551–18556
1183 (2010).

1184 6. Koo, D.-H. *et al.* Extrachromosomal circular DNA-based amplification and transmission of
1185 herbicide resistance in crop weed *Amaranthus palmeri*. *Proc. Natl. Acad. Sci.* **115**, 3332–3337
1186 (2018).

1187 7. Hull, R. *et al.* Transcription-induced formation of extrachromosomal DNA during yeast ageing.
1188 *PLoS Biol.* **17**, (2019).

1189 8. Shcheprova, Z., Baldi, S., Frei, S. B., Gonnet, G. & Barral, Y. A mechanism for asymmetric
1190 segregation of age during yeast budding. *Nature* **454**, 728–734 (2008).

1191 9. Nathanson, D. A. *et al.* Targeted therapy resistance mediated by dynamic regulation of
1192 extrachromosomal mutant EGFR DNA. *Science (80-.).* **343**, 72–76 (2014).

1193 10. Turner, K. M. *et al.* Extrachromosomal oncogene amplification drives tumour evolution and
1194 genetic heterogeneity. *Nature* **543**, 122–125 (2017).

1195 11. Møller, H. D. *et al.* Circular DNA elements of chromosomal origin are common in healthy human
1196 somatic tissue. *Nat. Commun.* **9**, 1–12 (2018).

1197 12. Shibata, Y. *et al.* Extrachromosomal MicroDNAs and Chromosomal Microdeletions in Normal
1198 Tissues. *Science (80-.).* **336**, 82–86 (2012).

1199 13. Durkin, K. *et al.* Serial translocation by means of circular intermediates underlies colour sidedness
1200 in cattle. *Nature* **482**, 81–84 (2012).

1201 14. Galeote, V. *et al.* Amplification of a Zygosaccharomyces bailii DNA segment in wine yeast
1202 genomes by extrachromosomal circular DNA formation. *PLoS One* **6**, 1–10 (2011).

1203 15. Selin, C., de Kievit, T. R., Belmonte, M. F. & Fernando, W. G. D. Elucidating the role of effectors in
1204 plant-fungal interactions: Progress and challenges. *Front. Microbiol.* **7**, 1–21 (2016).

1205 16. Dong, O. X. & Ronald, P. C. Genetic engineering for disease resistance in plants: Recent progress
1206 and future perspectives. *Plant Physiol.* **180**, 26–38 (2019).

1207 17. Sánchez-Vallet, A. *et al.* The Genome Biology of Effector Gene Evolution in Filamentous Plant
1208 Pathogens. *Annu. Rev. Phytopathol.* **56**, 21–40 (2018).

1209 18. Hollomon, D. W. Fungicide Resistance: 40 Years on and Still a Major Problem. *Springer* 3–11
1210 (2015). doi:10.1007/978-4-431-55642-8

1211 19. Fouché, S., Oggenfuss, U., Chanclud, E. & Croll, D. A devil's bargain with transposable elements in
1212 plant pathogens. *Trends Genet.* 1–9 (2021). doi:10.1016/j.tig.2021.08.005

1213 20. Bertazzoni, S. *et al.* Accessories Make the Outfit: Accessory Chromosomes and Other Dispensable
1214 DNA Regions in Plant-Pathogenic Fungi. *Mol. Plant-Microbe Interact.* **31**, 779–788 (2018).

1215 21. Croll, D. & McDonald, B. A. The accessory genome as a cradle for adaptive evolution in
1216 pathogens. *PLoS Pathog.* **8**, 8–10 (2012).

1217 22. Soanes, D. & Richards, T. A. Horizontal Gene Transfer in Eukaryotic Plant Pathogens. *Annu. Rev.*
1218 *Phytopathol.* **52**, 583–614 (2014).

1219 23. Dong, S., Raffaele, S. & Kamoun, S. The two-speed genomes of filamentous pathogens: Waltz
1220 with plants. *Curr. Opin. Genet. Dev.* **35**, 57–65 (2015).

1221 24. Dean, R. *et al.* The Top 10 fungal pathogens in molecular plant pathology. *Mol. Plant Pathol.* **13**,
1222 414–430 (2012).

1223 25. Fernandez, J. & Orth, K. Rise of a Cereal Killer: The Biology of Magnaporthe oryzae Biotrophic
1224 Growth. *Trends Microbiol.* **26**, 582–597 (2018).

1225 26. Foster, A. J. *et al.* CRISPR-Cas9 ribonucleoprotein-mediated co-editing and counterselection in
1226 the rice blast fungus. *Sci. Rep.* **8**, 1–12 (2018).

1227 27. Lanciano, S. *et al.* Sequencing the extrachromosomal circular mobilome reveals retrotransposon
1228 activity in plants. *PLoS Genet.* **13**, 1–20 (2017).

1229 28. Møller, H. D., Parsons, L., Jørgensen, T. S., Botstein, D. & Regenberg, B. Extrachromosomal
1230 circular DNA is common in yeast. *Proc. Natl. Acad. Sci.* **112**, E3114–E3122 (2015).

1231 29. Magdolen, V., Drubin, D. G., Mages, G. & Bandlow, W. High levels of profilin suppress the
1232 lethality caused by overproduction of actin in yeast cells. *FEBS Lett.* **316**, 41–47 (1993).

1233 30. Gladieux, P. *et al.* Coexistence of multiple endemic and pandemic lineages of the rice blast
1234 pathogen. *MBio* **9**, (2018).

1235 31. Zhong, Z. *et al.* Genetic Variation Bias toward Noncoding Regions and Secreted Proteins in the
1236 Rice Blast Fungus Magnaporthe oryzae. *mSystems* **5**, (2020).

1237 32. Wang, K. *et al.* Deciphering extrachromosomal circular DNA in Arabidopsis. *Comput. Struct.*
1238 *Biotechnol. J.* **19**, 1176–1183 (2021).

1239 33. Havecker, E. R., Gao, X. & Voytas, D. F. The diversity of LTR retrotransposons. *Genome Biol.* **5**,
1240 (2004).

1241 34. Dillon, L. W. *et al.* Production of Extrachromosomal MicroDNAs Is Linked to Mismatch Repair
1242 Pathways and Transcriptional Activity. *Cell Rep.* **11**, 1749–1759 (2015).

1243 35. Breier, A. M., Chatterji, S. & Cozzarelli, N. R. Prediction of Saccharomyces cerevisiae replication
1244 origins. *Genome Biol.* **5**, (2004).

1245 36. Wang, Z.-Q. *et al.* A Putative Zn2Cys6 Transcription Factor Is Associated With Isoprothiolane

1246 Resistance in Magnaporthe oryzae. *Front. Microbiol.* **9**, 2608 (2018).

1247 37. Bohnert, S. *et al.* Fungicide resistance toward fludioxonil conferred by overexpression of the
1248 phosphatase gene MoPTP2 in Magnaporthe oryzae. *Mol. Microbiol.* **111**, 662–677 (2019).

1249 38. Kim, K. *et al.* Evolution of the Genes Encoding Effector Candidates Within Multiple Pathotypes of
1250 Magnaporthe oryzae. **10**, 1–15 (2019).

1251 39. Latorre, S. M., Reyes-avila, C. S., Malmgren, A. & Win, J. Recently expanded clonal lineages of the
1252 rice blast fungus display distinct patterns of presence / absence of effector genes. 1–31 (2020).

1253 40. Borneman, A. R. *et al.* Whole-genome comparison reveals novel genetic elements that
1254 characterize the genome of industrial strains of saccharomyces cerevisiae. *PLoS Genet.* **7**, (2011).

1255 41. Foster, A. J., Jenkinson, J. M. & Talbot, N. J. Trehalose synthesis and metabolism are required at
1256 different stages of plant infection by Magnaporthe grisea. *EMBO J.* **22**, 225–235 (2003).

1257 42. Martin, M. Cutadapt removes adapter sequences from high-throughput sequencing reads.
1258 *EMBnet J.* **17**, 10–12 (2011).

1259 43. Bao, J. *et al.* PacBio Sequencing Reveals Transposable Elements as a Key Contributor to Genomic
1260 Plasticity and Virulence Variation in Magnaporthe oryzae. *Mol. Plant* **10**, 1465–1468 (2017).

1261 44. Dean, R. A. *et al.* The genome sequence of the rice blast fungus Magnaporthe grisea. *Nature* **434**,
1262 980–986 (2005).

1263 45. Li, H. Aligning sequence reads, clone sequences and assembly contigs with BWA-MEM. (2013).

1264 46. Li, H. Minimap2: Pairwise alignment for nucleotide sequences. *Bioinformatics* **34**, 3094–3100
1265 (2018).

1266 47. Min, B., Grigoriev, I. V. & Choi, I. G. FunGAP: Fungal Genome Annotation Pipeline using evidence-
1267 based gene model evaluation. *Bioinformatics* **33**, 2936–2937 (2017).

1268 48. Bao, W., Kojima, K. K. & Kohany, O. Repbase Update, a database of repetitive elements in
1269 eukaryotic genomes. *Mob. DNA* **6**, 4–9 (2015).

1270 49. Flynn, J. M. *et al.* RepeatModeler2 for automated genomic discovery of transposable element
1271 families. *Proc. Natl. Acad. Sci.* **117**, 9451–9457 (2020).

1272 50. Camacho, C. *et al.* BLAST+: architecture and applications. *BMC Bioinformatics* **10**, 421 (2009).

1273 51. Breen, J. *et al.* A highly conserved gene island of three genes on chromosome 3B of hexaploid
1274 wheat: diverse gene function and genomic structure maintained in a tightly linked block. *BMC*
1275 *Plant Biol.* **10**, 98 (2010).

1276 52. Thompson, J. D., Higgins, D. G. & Gibson, T. J. CLUSTAL W: improving the sensitivity of progressive
1277 multiple sequence alignment through sequence weighting, position-specific gap penalties and
1278 weight matrix choice. *Nucleic Acids Res.* **22**, 4673–4680 (1994).

1279 53. Smit, A., Hubley, R. & Green, P. RepeatMasker Open-4.0.

1280 54. Huang, W., Li, L., Myers, J. R. & Marth, G. T. ART: a next-generation sequencing read simulator.
1281 *Bioinformatics* **28**, 593–594 (2012).

1282 55. Ramírez, F. *et al.* deepTools2: a next generation web server for deep-sequencing data analysis.
1283 *Nucleic Acids Res.* **44**, W160–W165 (2016).

1284 56. Rice, P., Longden, L. & Bleasby, A. EMBOSS: The European Molecular Biology Open Software
1285 Suite. *Trends Genet.* **16**, 276–277 (2000).

1286 57. Zhang, W., Huang, J. & Cook, D. E. Histone modification dynamics at H3K27 are associated with
1287 altered transcription of in planta induced genes in Magnaporthe oryzae. *PLoS Genet.* **17**, 1–29
1288 (2021).

1289 58. Dobin, A. *et al.* STAR: ultrafast universal RNA-seq aligner. *Bioinformatics* **29**, 15–21 (2013).

1290 59. Grant, C. E., Bailey, T. L. & Noble, W. S. FIMO: scanning for occurrences of a given motif.
1291 *Bioinformatics* **27**, 1017–1018 (2011).

1292 60. Quinlan, A. R. & Hall, I. M. BEDTools: a flexible suite of utilities for comparing genomic features.
1293 *Bioinformatics* **26**, 841–842 (2010).

1294 61. Törönen, P., Medlar, A. & Holm, L. PANNZER2: a rapid functional annotation web server. *Nucleic*
1295 *Acids Res.* **46**, W84–W88 (2018).

1296 62. Alexa, A. & Rahnenfuhrer, J. topGO: Enrichment Analysis for Gene Ontology. (2019).

1297 63. Emms, D. M. & Kelly, S. OrthoFinder: Phylogenetic orthology inference for comparative
1298 genomics. *Genome Biol.* **20**, 1–14 (2019).

1299 64. Almagro Armenteros, J. J. *et al.* SignalP 5.0 improves signal peptide predictions using deep neural
1300 networks. *Nat. Biotechnol.* **37**, 420–423 (2019).

1301 65. Krogh, A., Larsson, B., Von Heijne, G. & Sonnhammer, E. L. L. Predicting transmembrane protein
1302 topology with a hidden Markov model: Application to complete genomes. *J. Mol. Biol.* **305**, 567–
1303 580 (2001).

1304 66. Sperschneider, J., Dodds, P. N., Gardiner, D. M., Singh, K. B. & Taylor, J. M. Improved prediction of
1305 fungal effector proteins from secretomes with EffectorP 2.0. *Mol. Plant Pathol.* **19**, 2094–2110
1306 (2018).

1307 67. Buchfink, B., Reuter, K. & Drost, H.-G. Sensitive protein alignments at tree-of-life scale using
1308 DIAMOND. *Nat. Methods* **18**, 366–368 (2021).

1309 68. Marçais, G. *et al.* MUMmer4: A fast and versatile genome alignment system. *PLoS Comput. Biol.*
1310 **14**, 1–14 (2018).

1311 69. Langner, T., Harant, A., Gomez-luciano, L. B., Shrestha, R. K. & Win, J. Genomic rearrangements
1312 generate hypervariable mini- chromosomes in host-specific lineages of the blast fungus. 1–34
1313 (2020).

1314 70. Slater, G. S. C. & Birney, E. Automated generation of heuristics for biological sequence
1315 comparison. *BMC Bioinformatics* **6**, 1–11 (2005).

1316 71. Tange, O. *GNU Parallel 2018*. (Ole Tange, 2018). doi:10.5281/zenodo.1146014

1317 72. Li, H. *et al.* The Sequence Alignment/Map format and SAMtools. *Bioinformatics* **25**, 2078–2079
1318 (2009).

73. pandas development team, T. pandas-dev/pandas: Pandas. (2020). doi:10.5281/zenodo.3509134

74. Harris, C. R. *et al.* Array programming with NumPy. *Nature* **585**, 357–362 (2020).

75. Virtanen, P. *et al.* SciPy 1.0: fundamental algorithms for scientific computing in Python. *Nat. Methods* **17**, 261–272 (2020).

76. Dowle, M. & Srinivasan, A. data.table: Extension of `data.frame`. (2020).

77. Wickham, H. tidyr: Tidy Messy Data. (2021).

78. Wickham, H. Reshaping Data with the reshape Package. *J. Stat. Softw.* **21**, 1–20 (2007).

79. Wickham, H., François, R., Henry, L. & Müller, K. dplyr: A Grammar of Data Manipulation. (2021).

80. Wickham, H. *ggplot2: Elegant Graphics for Data Analysis*. (Springer-Verlag New York, 2016).

81. Neuwirth, E. RColorBrewer: ColorBrewer Palettes. (2014).

82. Wickham, H. & Seidel, D. scales: Scale Functions for Visualization. (2020).

83. Wilke, C. O. cowplot: Streamlined Plot Theme and Plot Annotations for 'ggplot2'. (2020).

84. Slowikowski, K. ggrepel: Automatically Position Non-Overlapping Text Labels with 'ggplot2'. (2021).

85. Kassambara, A. ggpubr: 'ggplot2' Based Publication Ready Plots. (2020).

86. Hahne, F. & Ivanek, R. Statistical Genomics: Methods and Protocols. in (eds. Mathé, E. & Davis, S.) 335–351 (Springer New York, 2016). doi:10.1007/978-1-4939-3578-9_16

87. Iannone, R., Cheng, J. & Schloerke, B. gt: Easily Create Presentation-Ready Display Tables. (2021).

88. Hancks, D. C. & Kazazian, H. H. Roles for retrotransposon insertions in human disease. *Mob. DNA* **7**, (2016).